

Stable self-adaptive timestepping for Reduced Order Models for incompressible flows

Josep Plana-Riu^a, Henrik Rosenberger^{b,c}, Benjamin Sanderse^{b,c}, F.Xavier Trias^a

^aHeat and Mass Transfer Technological Centre, Technical University of Catalonia, Carrer de Colom 11, Terrassa, 08222, Spain

^bCentrum Wiskunde & Informatica, Science Park 123, Amsterdam, 1098 XG, the Netherlands

^cCentre for Analysis, Scientific Computing and Applications, Eindhoven University of Technology, PO Box 513, Eindhoven, 5600 MB, the Netherlands

Abstract

This work introduces RedEigCD, the first self-adaptive timestepping technique specifically tailored for reduced-order models (ROMs) of the incompressible Navier-Stokes equations. Building upon linear stability concepts, the method adapts the timestep by directly bounding the stability function of the employed time integration scheme using exact spectral information of matrices related to the reduced operators. Unlike traditional error-based adaptive methods, RedEigCD relies on the eigenbounds of the convective and diffusive ROM operators, whose computation is feasible at reduced scale and fully preserves the online efficiency of the ROM.

A central theoretical contribution of this work is the proof, based on the combined theorems of Bendixson and Rao, that, under linearized assumptions, the maximum stable timestep for projection-based ROMs is shown to be larger than or equal to that of their corresponding full-order models (FOMs).

Numerical experiments for both periodic and non-homogeneous boundary conditions demonstrate that RedEigCD yields stable timestep increases up to a factor 40 compared to the FOM, without compromising accuracy. The methodology thus establishes a new link between linear stability theory and reduced-order modeling, offering a systematic path towards efficient, self-regulating ROM integration in incompressible flow simulations.

Keywords: Computational Fluid Dynamics, Incompressible Navier-Stokes, Reduced-Order Modeling, Linear stability analysis, Self-adaptive time integration

1. Introduction

The numerical integration of nonlinear ordinary differential equations (ODEs), $\frac{d}{dt}\mathbf{u} = f(\mathbf{u}(t), t)$, like those arising from spatial discretization of the Navier-Stokes equations, requires setting the timestep of the integration. In the classical works of Hairer et al. [1], Butcher [2], this timestep, Δt , is generally assumed to be predetermined by the user, while later on, methods such as the Dormand-Price method (RKDP) [3] or Fehlberg (RKF) [4] were introduced to provide adaptive timestepping, based on truncation error estimates. As an alternative, the timestep Δt can also be determined by studying the stability of the linear system

$$\frac{d\mathbf{u}}{dt} = A\mathbf{u}, \quad (1)$$

where A follows from locally linearizing $f(\mathbf{u}(t), t)$. Restricting the product of the eigenbound of A , $\rho(A)$, and the timestep Δt to lie in the boundary of the stability region of the numerical time integration method thus maximizes the timestep when using an explicit time integration. Courant et al. [5] first introduced this concept in context of Computational Fluid Dynamics (CFD) with the development of the Courant-Friedrichs-Lewy (CFL) condition, where the stability condition is met by estimating the eigenvalues of the 1D convection-diffusion equation. Later on, this was generalized to the 3D Navier-Stokes equations by Trias and Lehmkuhl [6], where the timestep of the integration was modified each timestep to lie within the limit of the stability region of a second-order explicit multistep scheme. This was done by estimating the eigenvalues of the linearized system by means of the Gershgorin circle theorem. Later

works such as [7] improve the method by estimating the eigenbound of the linearized system without the need to fully reconstruct the matrix by exploiting its structure, thus making it more efficient.

Nonetheless, scale-resolving simulations, i.e., direct numerical simulation (DNS) and large-eddy simulation (LES), are generally prohibitively costly, especially for tasks that require many simulations such as control, design, optimization, or uncertainty quantification [8]. Hence, reduced-order models (ROMs) seek to alleviate the computational costs by projecting the high-dimensional system, also known as full-order model (FOM), to a reduced subspace [9–11], which depends on the construction of a basis. The methodology used for constructing this basis depends mostly on the characteristics of the problem, i.e., in an unsteady case where no parameters are involved, usually this basis is built as a set of Proper Orthogonal Decomposition (POD) modes from a matrix of snapshots [12–14], while in a case where the problem is parameter-based, this basis is built based on a (greedy) Reduced Basis algorithm [15, 16]. However, the procedure after constructing the basis is equivalent. For more details, the reader is referred to Lassila et al. [17].

Beyond timestep control at the FOM level, several contributions have addressed adaptive or stability-aware strategies in the reduced-order modeling framework. Amsallem and Farhat [18] proposed interpolation and stabilization techniques for parametric ROMs, emphasizing the importance of maintaining spectral consistency of the reduced operators. Their work highlighted the importance of maintaining consistency between the ROM and FOM eigenvalues to ensure numerical robustness. Nevertheless, this stabilization strategy does not explicitly link timestep adaptivity to linear stability theory, nor does it exploit the exact spectral information that can be computed efficiently at a reduced scale. Rezaian and Wei [19] demonstrated that analyzing and reassigning the eigenvalues of the reduced system's linear operator provides an effective means to control instability while preserving dominant dynamical features, establishing spectral analysis as a central tool for stability-aware model reduction.

Even though lots of efforts are devoted to pushing the boundaries of POD-Galerkin ROMs applied to CFD (closure models [20, 21], structure-preserving operators [22–24], hyper-reduction [23–26], stabilization [27–29], etc.), little effort has been made to finetune the timestep to maximize the "performance" of the time integration for these ROMs. Sanderse [8] indicated the use of the Gershgorin circle theorem as a possible way to estimate the eigenbounds of the combined reduced system to set the timestep, however no tests or implementation were presented. For structural mechanics, Bach et al. [30] performed an extensive analysis of the stability conditions for projection-based ROMs, where the maximum stable timesteps for both FOM and ROM were compared analytically. It was observed that the maximum stable timestep at the ROM level, assuming a linear problem, would not be smaller than the maximum stable timestep at the FOM level. To the best of our knowledge, such an analysis has not been performed for the nonlinear incompressible Navier-Stokes equations.

Therefore, this work aims to bridge the gap between self-adaptive timestepping techniques developed for scale-resolving CFD simulations [6, 7] and reduced-order models, as according to Bach et al. [30], it should be possible to generally obtain larger timesteps. Thus, the potential benefit of using a ROM is twofold: the reduced cost due to dimension reduction, and marching faster in time due to larger timesteps.

To extend existing self-adaptive timestepping methodologies to ROMs, the estimation of the eigenbounds should not break the leitmotif of reduced-order modeling [31]: online FOM-size operations should be avoided, in order to preserve the efficiency of the ROM compared to the FOM.

The present work introduces a new class of stability-driven self-adaptive timestepping algorithms for reduced-order models of the incompressible Navier-Stokes equations. The key novelty lies in (i) extending existing self-adaptive timestep control strategies - initially developed for full-order CFD solvers - to projection-based ROMs while fully preserving reduced-order efficiency, and (ii) establishing a theoretical proof, based on the combined theorems of Bendixson [32] and Rao [33], that the maximum stable timestep of a ROM is always larger or equal to that of its FOM counterpart. This connection between linear stability theory and reduced-order modeling has not been reported before for nonlinear incompressible flow systems. Furthermore, the proposed algorithm, termed RedEigCD, achieves stability control without resorting to full-order model operations. Lastly, it applies to both periodic and inflow-outflow configurations. Together, these elements form a novel stability-aware time-integration framework that advances the state-of-the-art in efficient and reliable ROM-based CFD simulations.

This article is organized as follows. In Section 2, the full-order model, the theory for linear stability analysis, and projection-based ROMs are introduced. In Section 3, our novel self-adaptive timestepping method for ROMs is presented, as well as an explanation why maximum stable timesteps for ROMs are generally larger than for their FOM counterparts. In Section 4, the novel self-adaptive timestepping method is tested in two test cases with different boundary conditions. Eventually, in Section 5, conclusions are drawn and future work is outlined.

2. Preliminaries: full-order model, linear stability analysis, and projection-based reduced-order model

2.1. Full-order model

The incompressible Navier-Stokes equations describe the behaviour of incompressible flows. In dimensionless form, they read

$$\nabla \cdot \mathbf{u} = 0, \quad (2a)$$

$$\frac{\partial \mathbf{u}}{\partial t} + (\mathbf{u} \cdot \nabla) \mathbf{u} = -\nabla p + \frac{1}{\text{Re}} \nabla^2 \mathbf{u} + \mathbf{f}, \quad (2b)$$

where $\mathbf{u} = \mathbf{u}(\mathbf{x}, t)$ is the flow velocity vector field, $p = p(\mathbf{x}, t)$ is the pressure scalar field, Re is the (constant and uniform) Reynolds number $\text{Re} = UL/\nu$, where U is a reference velocity, L is a reference lengthscale, and ν is the kinematic viscosity; and $\mathbf{f}(t)$ is the forcing term.

Following the notation of [34], after spatial discretization with a finite-volume method, the incompressible Navier-Stokes equations can be expressed in a semi-discrete formulation as

$$M\mathbf{u} = \mathbf{0}, \quad (3a)$$

$$\Omega \frac{d\mathbf{u}}{dt} + C(\mathbf{u})\mathbf{u} - D\mathbf{u} + \Omega G\mathbf{p} - \Omega \mathbf{f} = \mathbf{0}, \quad (3b)$$

where C is the convective operator, D is the diffusive operator, G is the gradient operator, \mathbf{f} is the discrete forcing term, and Ω is a diagonal matrix with the volumes of the cells as entries; \mathbf{u}, \mathbf{p} are the velocity and kinematic pressure. Note that this formulation can be easily adapted to methods that are not the finite-volume method. The exact form of these operators depends on the details of the chosen discretization. Within the framework of model order reduction, Eqs. (3a)-(3b) are identified as the FOM.

Eqs. (3a)-(3b) represent a system of differential-algebraic equations (DAE) of index 2, as the incompressibility condition is an algebraic constraint. Assuming no contribution from boundary conditions, this system reads as follows,

$$M\mathbf{u} = \mathbf{0}, \quad (4a)$$

$$\frac{d\mathbf{u}}{dt} = \tilde{F}(\mathbf{u}, t) - G\mathbf{p}, \quad (4b)$$

where $\tilde{F}(\mathbf{u}) = \Omega^{-1}(-C(\mathbf{u}) + D)\mathbf{u} + \mathbf{f}$.

From this point onwards, the discretization of the operators is assumed to be performed in a symmetry-preserving manner for the sake of simplicity. Symmetry-preserving schemes [34, 35] are a family of schemes that preserve the symmetry properties of the continuous operators at the discrete level. This is usually achieved by ensuring that the discrete gradient and divergence operators are dual to each other, i.e., $-\Omega M^T = G$; the convective operator is discretized in a skew-symmetric manner, and the diffusive operator is discretized as a symmetric matrix and corresponds to the composition of the gradient and divergence operators, resulting in a negative semi-definite matrix.

2.2. Linear stability analysis for the FOM

To integrate Eq.(3) in time, explicit one-step methods, such as any method of the explicit Runge-Kutta (ERK) family applied to projection methods [36], are considered. For further details on how this integration is performed in the context of the incompressible Navier-Stokes equations, the reader is referred to [37]. A similar methodology for explicit multi-step methods, such as the second-order Adams-Bashforth (AB2), is developed in [6].

For a general ERK applied to Eq.(3), the methodology can be contracted to

$$\mathbf{u}^{n+1} \approx R(\Delta t F)\mathbf{u}^n, \quad (5)$$

where $F = \Omega^{-1}(D - C(\mathbf{u})) \in \mathbb{R}^{m \times m}$ is the operator arising from linearizing $\tilde{F}(\mathbf{u})$ in Eq.(4), and $R(z)$ is the stability (or augmentation) function of the given (linearized) scheme. Note that there is an approximation symbol instead of an equal symbol as the $n + 1$ value requires projecting every stage in the set of incompressible velocity fields [37, 38], which is left out in Eq.(5). However, the projection step in a projection method is implicit and does not affect the stability region.

Following linear stability analysis theory for differential equations, the linear method is stable [39] if

$$\|R(\Delta t F)\|_2 \leq 1. \quad (6)$$

As explained in [39], this requirement can be equivalently expressed on the largest in magnitude eigenvalue λ_F of F ,

$$|R(\Delta t \lambda_F)| \leq 1. \quad (7)$$

The maximum stable timestep for a Runge-Kutta integration is such that, for $z_{max} = \Delta t \|\lambda_F\|$, it fulfills the equation $\|R(z_{max})\| = 1$. By doing so, the eigenvalue $\Delta t \lambda_F$ is placed over the stability region (Figure 1). z_{max} is obtained by solving $\|R(z)\| - 1 = 0$ using a bisection method along the axis defined by the origin of coordinates $(0 + 0i)$ and λ_F every timestep. Hence, the self-adaptive timestep can be computed as

$$\Delta t = \frac{z_{max}}{\|\lambda_F\|}. \quad (8)$$

Thus, in general, the goal of any self-adaptive timestepping method is to calculate (or estimate) the eigenbounds of F so that the maximum stable timestep is computed using Eq.(8).

The methodology explained in this subsection assumes the discretization is symmetry-preserving. The reader is referred to Appendix B of [7] to generalize the method to non-symmetry-preserving schemes, such as upwinding schemes, by splitting the convective operator in its symmetric and skew-symmetric contributions.

As explained in Section 2.1, the symmetry-preserving discretization ensures that certain property from the continuous operators are preserved [35]: a symmetry-preserving diffusive operator is represented by a real semi-negative definite symmetric matrix, and the convective operator is represented by a real skew-symmetric matrix [34, 35]. Hence, the eigenvalues of the former lie on the negative real axis in the complex plane, while the eigenvalues of the latter lie on the imaginary axis. As eigenbounds are subadditive, i.e. $\rho(A + B) \leq \rho(A) + \rho(B)$, where $\rho(A)$ determines the eigenbounds of the matrix A , the eigenbound of the operator F , λ_F , lies, according to Bendixson's inequality [32], in the rectangle defined by the eigenbounds of the convective and diffusive operators as shown in Figure 1.

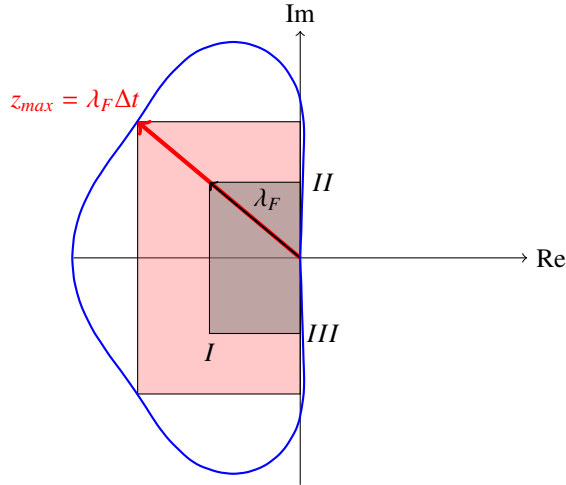


Figure 1: Schematic illustration of Bendixson's rectangle (gray) [6] for the eigenvalues of F . $I : \rho(\Omega^{-1}D)$, $II : \rho(\Omega^{-1}C(\mathbf{u}))$, $III : -\rho(\Omega^{-1}C(\mathbf{u}))$. The red rectangle represents the stability region bounds. The blue curve represents the boundary of the stability region for a third-order Runge-Kutta scheme.

The stability region is determined by the timestepping scheme. For ERK schemes defined by the coefficients $A = [a_{ij}]_{i,j=1:s}$ and $\mathbf{b} = (b_1 \ b_2 \ \dots \ b_s)^T$, with s stages [40], if $s \leq 4$ and the order of accuracy $p = s$, the stability function is the Taylor polynomial of e^z up to the number of stages [1],

$$R(z) = 1 + \sum_{j=1}^s \frac{1}{j!} z^j, \quad (9)$$

which makes the implementation much easier to test. Moreover, the most widely used RK schemes: Heun's 2nd- and

3rd-order schemes, Kutta's 3rd order scheme, the classic 4th-order scheme; satisfy this condition of $s = p \leq 4$.

2.3. Existing self-adaptive timestepping techniques for the FOM

As previously detailed, the goal of a self-adaptive timestepping technique is determining the eigenbounds of the operators as accurately as possible, given that the exact computation of the eigenvalues is prohibitive for a classical FOM problem size, which can reach up to several billion unknowns.

EigenCD [6] estimates the eigenbounds by making use of the Gershgorin circle theorem [41], which is relatively inexpensive compared to the exact computation of the eigenvalues, while simultaneously providing a relatively accurate bound so that it allows having a much larger timestep than the original CFL condition [5]. To do so, the method relies on the explicit construction of the convective and diffusive operators at every timestep, which allows the application of the Gershgorin circle theorem to both matrices to compute the eigenbounds of the operators.

In contrast to EigenCD, AlgEigCD [7] exploits the structure of the convective and diffusive operators to estimate the eigenbounds without explicitly constructing these operators. On a collocated grid, the duality of the gradient and the divergence, and the definition of the interpolation of the velocity at the faces for a symmetry-preserving scheme allows the (offline) computation of a matrix depending only on the incidence matrices as well as Ω . Therefore, the eigenbounds are computed online by simply performing a matrix-vector product of this offline-computed matrix with the diffusive and convective fluxes. This construction, opposite to the one from EigenCD, allows simplifying the estimation of the eigenbound to a sparse matrix-vector product, where the sparse matrix has been computed *a priori*. This allows making the eigenbound estimation much more efficient.

The main question in this article is whether the EigenCD/AlgEigCD method can also be applied in a reduced-order model context. For this purpose, the reduced-order model framework is introduced in the following subsection.

2.4. Energy-conserving POD-Galerkin method

The ROM considered in this work follows the ODE-based projection approach [42], where the PDE is first discretized in space, as in Eq. (3), and afterwards is projected to the subspace obtained with POD [8].

Let the velocity vector be defined as $\mathbf{u} \in \mathbb{R}^{N_v}$, and the POD-Galerkin approximation is obtained by the Ansatz that the velocity field can be approximated by

$$\mathbf{u}_c(t) \approx \mathbf{u}_r(t) \equiv \Phi \mathbf{a}(t), \quad (10)$$

where $\Phi \in \mathbb{R}^{N_v \times M}$ is the projection matrix, and $\mathbf{a}(t) \in \mathbb{R}^M$ is the coefficient vector; assuming $M \ll N_v$. In this work, the basis is obtained from the so-called snapshot matrix X which contains K snapshots of the velocity field, $X = [\mathbf{u}_c^1 \dots \mathbf{u}_c^n \dots \mathbf{u}_c^K] \in \mathbb{R}^{N_v \times K}$, obtained from a (so-called 'offline') solution of the FOM from Eq. (3).

The construction of the POD basis is performed using a weighted orthonormality condition, $\Phi^T \Omega \Phi = I_M$, where I_M is the identity matrix of size M , which is consistent with the inner product of the velocity as well as the ROM kinetic energy equation [8]. As AlgEigCD provides an efficient way to integrate the FOM using variable timesteps, it is important to construct the POD basis by considering that there is a variable timestep [43]. This is taken into account in the construction of the POD basis as described in Appendix A.

Given Φ , and the Ansatz, both mass and momentum equations from Eq. (3) can be projected [22] to obtain the reduced-order equations. Concerning the conservation of mass, this is preserved automatically if the snapshots are divergence free ($M X_j = 0$), regardless of \mathbf{a} .

First, consider a case with homogeneous boundary conditions. Concerning the conservation of momentum, the ROM momentum equation is given by

$$\frac{d\mathbf{a}}{dt} = -\Phi^T C(\Phi \mathbf{a}_c) \Phi \mathbf{a} + \Phi^T D \Phi \mathbf{a}, \quad (11)$$

where the weighted orthonormality condition has been applied. \mathbf{a} stands for the convected velocity in the reduced space while $\mathbf{a}_c = \mathbf{a}$ stands for the convecting velocity in the reduced space. Applying the duality of the divergence and gradient operators inherent in a symmetry-preserving discretization, the pressure term is exactly zero, and can be dropped if the snapshots are divergence-free [8], as shown by

$$\Phi^T G \mathbf{p} = -\Phi^T \Omega M^T \mathbf{p} = (M \Omega \Phi)^T \mathbf{p} = 0. \quad (12)$$

In the current setup, building the reduced convective operator in an online phase would rely on operations at the FOM level, which would notably deteriorate the performance of the ROM. Following Stabile and Rozza [31], the reduced convective term can be rewritten as

$$\Phi^T C(\Phi \mathbf{a}_c) \Phi \mathbf{a} \equiv \underbrace{[\Phi^T C(\Phi_1) \Phi \ C_{r,2} \ \dots \ C_{r,M}]}_{C_{r,1}} (\mathbf{a}_c \otimes \mathbf{a}) = C_r(\mathbf{a}_c \otimes \mathbf{a}) = \left(\sum_{i=1}^M a_{c,i} C_{r,i} \right) \mathbf{a}. \quad (13)$$

With this approach, all the reduced convective matrices $C_{r,i}$ can be computed offline in a setup phase that keeps the complexity of online operations at ROM level, while all FOM-size operations are performed offline (only once).

Hence, the ROM derived in Eq.(11) can be written as

$$\frac{d\mathbf{a}}{dt} = -C_r(\mathbf{a}_c \otimes \mathbf{a}) + D_r \mathbf{a} + F_{r,0}, \quad (14)$$

which has a complexity of $\mathcal{O}(M^3)$. In many cases, the required number of modes M is low enough so that performing operations of this complexity is acceptable. For larger M , hyperreduction techniques such as the discrete empirical interpolation method might be used [23–25] that reduce the complexity to $\mathcal{O}(M^2)$.

In the case of non-homogeneous boundary conditions, a linear term arising from the convective term interaction with the boundary conditions should be added to Eq.(14) [22]. To consider the presence of non-homogeneous boundary conditions, the contribution from these non-homogeneous boundary conditions ($\mathbf{u}_{\text{inhom}}$) has to be added to the ansatz. Therefore,

$$\mathbf{u}_r(t) = \Phi \mathbf{a}(t) + \mathbf{u}_{\text{inhom}}(t), \quad (15)$$

where $\mathbf{u}_{\text{inhom}}$ is the lifting function defined by Rosenberger and Sandeher [22]. As explained in Appendix B in [8], the Navier-Stokes equations with inhomogeneous boundary conditions are given by

$$M\mathbf{u} = \mathbf{y}_M \quad (16)$$

$$\Omega \frac{d\mathbf{u}}{dt} = -K((\Pi \mathbf{u} + \mathbf{y}_\Pi) \circ (A\mathbf{u} + \mathbf{y}_A)) + (D\mathbf{u} + \mathbf{y}_D) - (\Omega G\mathbf{p} + \mathbf{y}_G) + \mathbf{f}, \quad (17)$$

where Π interpolates the fluxes to the staggered faces, and A interpolates the velocities to the staggered faces. As described in [44], the boundary contributions \mathbf{y}_* , $*$ $\in \{A, D, \Pi, G, M\}$ can be expressed as linear functions of a vector \mathbf{y}_{bc} that fully describes the prescribed boundary conditions, $\mathbf{y}_* = B_* \mathbf{y}_{bc}$. The boundary condition vector is approximated as $\mathbf{y}_{bc}(t) \approx \Phi_{bc} \mathbf{a}_{bc}(t)$, where $\mathbf{a}_{bc} \in \mathbb{R}^{M_{bc}}$, and M_{bc} being the number of modes used for the boundary conditions. Inserting this approximation and the Ansatz (15) with $\mathbf{u}_{\text{inhom}}(t) = F_{\text{inhom}} \mathbf{a}_{bc}(t)$ into (17) (projected onto Φ), leads to

$$\begin{aligned} \frac{d\mathbf{a}}{dt} = \Phi^T \Big[& -K((\Pi \Phi \mathbf{a}_c + (\Pi B_{\text{inhom}} + B_\Pi \Phi_{bc}) \mathbf{a}_{bc}) \circ (A \Phi \mathbf{a} + (A B_{\text{inhom}} + B_A \Phi_{bc}) \mathbf{a}_{bc})) \\ & + (D \Phi \mathbf{a} + (D B_{\text{inhom}} + B_D \Phi_{bc}) \mathbf{a}_{bc}) - B_G \Phi_{bc} \mathbf{a}_{bc} + \mathbf{f}_c \Big]. \end{aligned} \quad (18)$$

Here, $\Phi^T G_c \mathbf{p}_c = 0$ has already been eliminated. The convection operator can be decomposed into a term quadratic in \mathbf{a} ,

$$-\Phi^T K((\Pi \Phi \mathbf{a}_c) \circ (A \Phi \mathbf{a})) =: C_{\text{hom}}(\mathbf{a}_c \otimes \mathbf{a}), \quad (19)$$

a term linear in both, \mathbf{a} and \mathbf{a}_{bc} ,

$$-\Phi^T K((\Pi \Phi \mathbf{a}) \circ ((A B_{\text{inhom}} + B_A \Phi_{bc}) \mathbf{a}_{bc})) - K(((\Pi B_{\text{inhom}} + B_\Pi \Phi_{bc}) \mathbf{a}_{bc}) \circ (A \Phi \mathbf{a})) =: C_{\text{hom,bc}}(\mathbf{a} \otimes \mathbf{a}_{bc}), \quad (20)$$

and a term quadratic in \mathbf{a}_{bc} ,

$$-\Phi^T K(((\Pi B_{\text{inhom}} + B_\Pi \Phi_{bc}) \mathbf{a}_{bc}) \circ ((A B_{\text{inhom}} + B_A \Phi_{bc}) \mathbf{a}_{bc})) =: C_{bc}(\mathbf{a}_{bc} \otimes \mathbf{a}_{bc}). \quad (21)$$

Therefore, with the additional terms from Eqs.(19)-(21), the ROM reads

$$\frac{d\mathbf{a}}{dt} = -C_{\text{hom}}(\mathbf{a}_c \otimes \mathbf{a}) - C_{\text{hom,bc}}(\mathbf{a} \otimes \mathbf{a}_{bc}) - C_{bc}(\mathbf{a}_{bc} \otimes \mathbf{a}_{bc}) + D_r \mathbf{a} + F_{r,0}. \quad (22)$$

Therefore, considering Eq. (22), the linear contribution from the convective term in \mathbf{a} is

$$C_l(t) = \frac{\partial C_{\text{hom,bc}}(\mathbf{a} \otimes \mathbf{a}_{bc})}{\partial \mathbf{a}} = C_{\text{hom,bc}}(I_M \otimes \mathbf{a}_{bc}(t)) = [C_{\text{hom,bc},1} \dots C_{\text{hom,bc},M}](I_{M_{bc}} \otimes \mathbf{a}_{bc}(t)) = \sum_{i=1}^{M_{bc}} a_{bc,i}(t) C_{l,i}, \quad (23)$$

where $C_{\text{hom,bc}} \in \mathbb{R}^{M \times M M_{bc}} = [C_{\text{hom,bc},1} \dots C_{\text{hom,bc},M}]$ is the matrix containing the reduced contribution of the boundary conditions to the convective term, and $\mathbf{a}_{bc}(t) \in \mathbb{R}^{M_{bc}}$ are the coefficients of the boundary condition at time t [22].

3. Generalizing the self-adaptive timestep methods for ROMs

3.1. Estimating the eigenbound of the reduced operators

As for FOMs discussed in Section 2.3, the crucial element of self-adaptive timestepping methods for ROMs is the computation of eigenbounds. Since the convection operator depends on the current velocity, these eigenbounds must be computed for every timestep. To preserve the efficiency gain achieved by the adaptive timestepping, the computational costs of this eigenbound computation should be negligible compared to the overall costs of the numerical simulation. As described in Section 2.4, the simulation of each timestep has computational costs of $O(M^3)$ if the convection term is computed exactly, and of $O(M^2)$ if hyperreduction is used. Although the present work focuses on the standard projection without hyperreduction (in order to ensure exact energy conservation and stability properties), we keep the requirement that the computational cost for computing the eigenbounds at each time step should be at most $O(M^2)$.

The exact computation of the eigenvalues of a matrix in $\mathbb{R}^{M \times M}$ has computational costs of $O(M^3)$ [45–47] which is too expensive for practical purposes. As an alternative, Gershgorin’s circle theorem can be applied to the reduced operators as in EigenCD [6] to estimate the eigenbounds. This approach has costs in $O(M^2)$ so still might contribute significantly to the overall costs. Moreover, this estimate can be quite inaccurate and hence result in timesteps significantly smaller than the largest stable timestep based on the exact eigenbounds. Another alternative is AlgEigCD [7], which was proposed on the FOM level and leverages the structure of the convective and diffusive operators. A natural question that we will address now is whether this method can be transferred to the ROM level.

The concept behind AlgEigCD is approximating the eigenbounds of the operators by finding a factorization $H = AB$ such that the eigenbound of $A^T B^T$ can be approximated efficiently. The reduced operators, however, have the form $H = \Phi^T H_F$, where H_F is a matrix with FOM dimensions. Following AlgEigCD, the eigenbound of a matrix H would be obtained by approximating the eigenbounds of $H^* = (\Phi^T A_F)^T (B_F \Phi)^T$, where $A_F B_F$ is a factorization of H_F . In contrast to H , H^* is a matrix of FOM dimension, therefore the eigenbound estimation for H^* is more expensive than for H itself.

Thus, such a transfer does not result in an efficient method. Instead, we will propose a new approach that exploits the structure of the reduced operators (13) and (23).

Concerning the diffusive operator, the application of the exact calculation of the eigenvalues is straightforward, as the diffusive operator at the ROM level is built as $\Phi^T D \Phi$, and it is a real symmetric matrix. Thus, its eigenvalues are real, and the eigenbound $\rho(D_r)$ can be computed exactly in an offline stage.

On the other hand, the convective operator at the ROM level is built as in Eq. (13). Simplifying the momentum equation as a particular case of a convection-diffusion equation with predefined convecting velocity, the Jacobian of the convective operator with respect to the convected velocity coefficients reads as

$$J_C = \frac{\partial C_r}{\partial \mathbf{a}} = \sum_{i=1}^M a_{c,i} C_{r,i}, \quad (24)$$

which yields a skew-symmetric Jacobian iff $C_{r,i}$ is skew-symmetric for all i . Appendix C shows the computation of the Jacobian of the convective term for a general convection-diffusion equation. Thus, the linearized form that is used for the linear stability analysis corresponds to

$$\sum_{i=1}^M a_{c,i} C_{r,i}. \quad (25)$$

Note that at every timestep \mathbf{a}_c changes, yet $C_{r,i}$ does not as it only depends on Φ_i . Thus, the eigenbound of the reduced convective operator can be estimated by employing the property that eigenbounds are subadditive. Hence,

the eigenbound of the reduced convective operator can be bound as

$$\rho(C_r) \leq \sum_{i=1}^M |a_{c,i}| \rho(C_{r,i}), \quad (26)$$

where $\rho(C_{r,i})$ is calculated exactly in an offline stage, as its complexity of $O(M^3)$ can be tolerated. However, the online complexity to compute Eq.(26) is just $O(M)$, as it corresponds to a dot product. This complexity is negligible compared to the $O(M^3)$ cost of evaluating the ROM every timestep (Eq.(14)).

In case of non-homogeneous boundary conditions, the ROM additionally contains a linear convective term which is in general neither skew-symmetric nor symmetric [22]. Given that this term is time-dependent in case of time-dependent boundary conditions, its eigenvalues should be estimated at every timestep. As the non-homogeneous boundary conditions contributions are neither symmetric nor skew-symmetric in general, they are split into their symmetric and skew-symmetric contributions, i.e.,

$$C_{l,i}^S = \frac{1}{2}(C_{l,i} + C_{l,i}^T), \quad (27a)$$

$$C_{l,i}^\Omega = \frac{1}{2}(C_{l,i} - C_{l,i}^T). \quad (27b)$$

Therefore, the symmetric term contributes to the real bound, while the skew-symmetric term affects the imaginary bound.

The linear contribution (Eq.(23)) has the same structure as the convective operator (Eq.(13)). Therefore, the same approach can be used to estimate the eigenbounds for the symmetric and skew-symmetric terms, which leads to

$$\rho(C_l^S(t)) \leq \sum_{i=1}^{M_{bc}} |a_{bc,i}(t)| \rho(C_{l,i}^S), \quad (28a)$$

$$\rho(C_l^\Omega(t)) \leq \sum_{i=1}^{M_{bc}} |a_{bc,i}(t)| \rho(C_{l,i}^\Omega), \quad (28b)$$

where $\rho(C_{l,i}^S)$ and $\rho(C_{l,i}^\Omega)$ are computed exactly in an offline stage, and $\mathbf{a}_{bc}(t)$ is already known at every timestep. Similarly to Eq.(26), the online complexity of these estimations is $O(M_{bc})$.

Hence, this new approach to estimate the eigenbounds used to determine the largest stable timestep is determined by

$$\Re(\lambda_F) \leq \tilde{\Re}(\lambda_F) := \rho(D_r) + \sum_{i=1}^{M_{bc}} |a_{bc,i}(t)| \rho(C_{l,i}^S), \quad (29a)$$

$$\Im(\lambda_F) \leq \tilde{\Im}(\lambda_F) := \sum_{i=1}^M |a_{c,i}| \rho(C_{r,i}) + \sum_{i=1}^{M_{bc}} |a_{bc,i}(t)| \rho(C_{l,i}^\Omega). \quad (29b)$$

With all these ingredients, the stability-aware self-adaptive timestep method for ROMs, RedEigCD, can be summarized in Algorithm 1, where T is the simulation end time.

Finally, the operational differences between the proposed framework and existing strategies is presented. Table 1 presents a side-by-side comparison of EigenCD, AlgEigCD, and RedEigCD, focusing on their algorithmic complexity and applicability to ROM simulations.

3.2. Analytical stability analysis of ROMs

In practice, it has been observed that ROMs are stable for larger timesteps than the FOM. For instance, Baiges et al. [48] indicated that for explicit time integration schemes, the timestep was not restricted by the CFL condition, opposite to the FOM. Intuitively, cutting off some of the highest (spatial) frequencies, which are represented by the smallest singular values, would imply removing some of the most rapid (temporal) modes. These are the modes that make the system stiffer, and thus are the most restrictive modes in terms of stability. By eliminating these modes, the stability constraint is more relaxed, and the method yields, as a consequence, larger timesteps in the reduced framework.

Algorithm 1 Stability-aware self-adaptive timestep method for ROMs (RedEigCD)

Offline stage:

- 1: Compute Φ from snapshots.
- 2: Compute D_r as $\Phi^T D \Phi$.
- 3: Compute $C_{r,i}$ as in Eq.(13) for $i = 1, \dots, M$.
- 4: Compute $C_{l,i}$ as in Eq.(23) for $i = 1, \dots, M_{bc}$.
- 5: ★ Compute $\rho(D_r)$ and $\rho(C_{r,i})$ for $i = 1, \dots, M$.
- 6: ★ Compute $\rho(C_{l,i}^S)$ and $\rho(C_{l,i}^\Omega)$ for $i = 1, \dots, M_{bc}$.

Online stage:

- 1: Set $t = 0$, $\mathbf{a} = \mathbf{a}_0$, $\Delta t = \Delta t_0$.
 - 2: **while** $t < T$ **do**
 - 3: ★ Compute $\tilde{\mathbf{R}}(\lambda_F)$ and $\tilde{\mathbf{J}}(\lambda_F)$ as in Eq.(29).
 - 4: ★ Compute z_{max} with the bisection method.
 - 5: ★ Compute Δt as in Eq.(8).
 - 6: Advance Eq.(14) in time with the chosen time integration scheme.
 - 7: $t = t + \Delta t$
 - 8: **end while**
- ★ Steps required for a self-adaptive time integration with RedEigCD.
-

Table 1: Description and comparison of computational complexity (offline vs. online) for EigenCD, AlgEigCD, and the proposed RedEigCD method.

| Method | Description | Online complexity | Offline complexity |
|---------------------|--|-------------------|--------------------|
| EigenCD [6] | Applies Gershgorin to the explicit $D_r, C_r(\mathbf{a})$ operators. Inaccurate for dense matrices in a reduced framework. | $O(M^2)$ | 0 |
| AlgEigCD [7] | Relies on the structure of $D_r, C_r(\mathbf{a})$ to reduce the eigenvalue computation to a matrix-vector product of FOM size. | $O(N_F)$ | $O(N_F)$ |
| RedEigCD (proposed) | Uses the tensorial decomposition to simplify the eigenvalue calculation for $C_r(\mathbf{a})$. Uses the exact eigenvalues for D_r . | $O(M)$ | $O(M^3)$ |

Bach et al. [30] analyzed the stability of ROMs compared to FOMs for linear elasticity problems, which are linear problems with real symmetric matrices (like diffusion), where the timestep at the ROM level is demonstrated to be at least as large as the timestep at the FOM level, yet usually larger.

To provide a mathematical foundation to this qualitative point of view, Bach et al. [30] made use of the Poincaré separation theorem, which reads as follows:

Lemma 1. (Poincaré separation theorem [49, 50]) *Let $V \in \mathbb{R}^{m \times k}$, where $k \ll m$, be a matrix with orthonormal column vectors, i.e. $V^T V = I_k$. Let $A \in \mathbb{R}^{m \times m}$ be a real symmetric matrix. Then, the eigenvalues of $V^T A V$ separate the eigenvalues of A such that*

$$\lambda_i \leq \tilde{\lambda}_i \leq \lambda_{m-k+i}, \quad i \leq k \quad (30)$$

where λ_i denotes the eigenvalues of A , and $\tilde{\lambda}_i$ the eigenvalues of $V^T A V$, ordered in increasing order, $\lambda_1 \leq \lambda_2 \leq \dots \leq \lambda_m$ and $\tilde{\lambda}_1 \leq \tilde{\lambda}_2 \leq \dots \leq \tilde{\lambda}_k$ respectively.

At the limit, $i = k$, the value $\tilde{\lambda}_k$ denotes the eigenbound of $V^T A V$. According to Lemma 1, $\tilde{\lambda}_k$ lies in the range $[\lambda_k, \lambda_m]$. Therefore, $\tilde{\lambda}_k \leq \lambda_m$, which determines the eigenbound of A . For the sake of clarity, this has been represented graphically in Figure 2. This theorem can be applied straightaway to the diffusive operator and shows that $\rho(D_r) \leq \rho(D)$ as the diffusive operator corresponds to a real symmetric matrix, and Φ is an Ω -orthonormal matrix. Therefore,

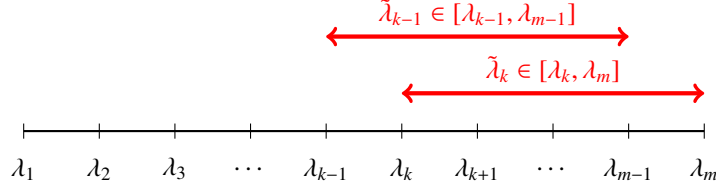


Figure 2: Graphical representation of the range of reduced eigenvalues for $i = k$ and $i = k - 1$, in red, according to the Poincaré separation theorem.

Lemma 1 holds, as Bach et al. [30] showed that its result is not altered if the basis fulfills $V^T \Omega V = I_k$ instead of $V^T V = I_k$.

In contrast, Lemma 1 cannot be applied to the convective term as it is not symmetric. Therefore, the work of Bach et al. [30] is extended to the case of ROMs with non-symmetric operators. To do so, the work of Rao [33] is employed, which extends the Poincaré separation theorem to singular values instead of eigenvalues, and thus holds even for the case of non-symmetric matrices.

Lemma 2. (Poincaré separation theorem for singular values [33]) Let $A \in \mathbb{R}^{m \times n}$. Let $B \in \mathbb{R}^{m \times k}$ and $C \in \mathbb{R}^{n \times r}$ be orthonormal matrices, i.e. $B^T B = I_k$ and $C^T C = I_r$. The i -th singular value of A is denoted by σ_i in increasing order, as for the Poincaré separation theorem. Moreover, $\tilde{\sigma}_i$ denotes the i -th singular value of $B^T A C$. Then, the following inequality holds:

$$\sigma_i \leq \tilde{\sigma}_i \leq \sigma_{\tilde{m}-i+1}, \text{ for } 1 \leq i \leq \min(r, k), \quad (31)$$

where $\tilde{m} = \min(m, n)$.

Let, then, A be a square matrix and $B = C$. In the current case, $A = C(\mathbf{u})$, and $B = \Phi$. Hence, this theorem can be applied to the convective term by making use of the fact that the singular values of a real skew-symmetric matrix correspond to the absolute values of the eigenvalues, which suffices to estimate the eigenbound of the operator.

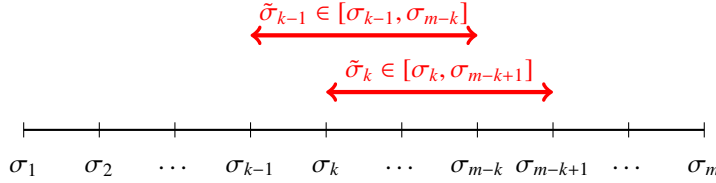


Figure 3: Graphical representation of the range of reduced singular values for $i = k$ and $i = k - 1$, in red, according to the Poincaré separation theorem for singular values.

Hence, the inequality can be rewritten for $r = k$, $m = n$ with $i = k$ to estimate the eigenbound of the convective term, which reads as follows,

$$\sigma_k \leq \tilde{\sigma}_k \leq \sigma_{m-k+1} \leq \sigma_m, \quad (32)$$

as graphically represented in Figure 3. Compared to Lemma 1, Eq.(32) does include the inequality $\sigma_{m-k+1} \leq \sigma_m$, as Lemma 2 bounds the singular values of the reduced matrix with σ_k and σ_{m-k+1} as shown in Fig. 2, yet by the assumed order of the singular values $\sigma_{m-k+1} \leq \sigma_m$. As the convective operator is represented by a skew-symmetric matrix, it is a normal matrix, i.e. $C^* C = C C^*$, and thus the results in terms of singular values can be translated to eigenvalues according to Lemma 3. Thus, the eigenvalues of $C(\mathbf{u})$ are greater than those of $C_r(\mathbf{a})$. Therefore, $\rho(C_r) \leq \rho(C)$.

Lemma 3. Let $A \in \mathbb{C}^{n \times n}$ be a normal matrix (i.e. $A^* A = A A^*$). Let $\lambda_1, \dots, \lambda_n$ be the eigenvalues of A , listed with algebraic multiplicity. Let $\sigma_1, \dots, \sigma_n$ be the singular values of A (the nonnegative square roots of the eigenvalues of $A^* A$), also listed with multiplicity. Then, the singular values are the absolute values of the eigenvalues:

$$\{\sigma_1, \dots, \sigma_n\} = \{|\lambda_1|, \dots, |\lambda_n|\}. \quad (33)$$

Proof. As A is a normal matrix, it can be diagonalized with a unitary matrix U , which is a set of orthonormal eigenvectors such that $U^* U = I$, and a diagonal matrix Λ , which has the eigenvalues of A as entries, i.e. $\Lambda = \text{diag}(\lambda_1, \dots, \lambda_n)$

[51, pp. 101–103]. Therefore,

$$A = U\Lambda U^*. \quad (34)$$

Then, A^*A can be written as

$$A^*A = (U\Lambda U^*)^*(U\Lambda U^*) = U\Lambda^*U^*U\Lambda U^* = U\Lambda^*\Lambda U^*, \quad (35)$$

where $\Lambda^*\Lambda = \text{diag}(\lambda_1^*\lambda_1, \dots, \lambda_n^*\lambda_n) = \text{diag}(|\lambda_1|^2, \dots, |\lambda_n|^2)$. Therefore,

$$A^*A = U\text{diag}(|\lambda_1|^2, \dots, |\lambda_n|^2)U^*. \quad (36)$$

Then, the i -th column of U , \mathbf{u}_i , is going to be an eigenvector of A^*A with eigenvalue $|\lambda_i|^2$, since $A^*A\mathbf{u}_i = \mathbf{u}_i|\lambda_i|^2$. By definition, the singular values of A are the eigenvalues of A^*A . Therefore, it shows that Eq.(33) holds and, with a proper reordering,

$$\sigma_i = |\lambda_i|, \quad \forall i. \quad (37)$$

□

As Eq.(29) indicates, the magnitude of the relevant eigenvalue in the ROM is determined by the contributions of both diffusive and convective term. Thus, the following theorem can be stated.

Theorem 1. *Let Δt^{ROM} be the largest stable timestep for the ROM given a state \mathbf{a} , and Δt^{FOM} the largest stable timestep for a state \mathbf{u} that is in the span of Φ , e.g. $\mathbf{u} = \Phi\mathbf{a}$, both using the same explicit time integration scheme. Then, $\Delta t^{\text{ROM}} \geq \Delta t^{\text{FOM}}$.*

Proof. Let $\lambda_{F,\text{FOM}} = \rho(D) + i\rho(C(\mathbf{u}))$ be the eigenvalue of the FOM, and $\lambda_{F,\text{ROM}}$ be calculated as in Eq.(29). As shown above, $\rho(D_r) \leq \rho(D)$ (Lemma 1). Moreover, given $\mathbf{u} = \Phi\mathbf{a}$ is the FOM equivalent of \mathbf{a} , $\rho(C_r) \leq \rho(C)$ (Lemma 2). Therefore, $\|\lambda_{F,\text{FOM}}\| \geq \|\lambda_{F,\text{ROM}}\|$, where $\|\cdot\|$ denotes the complex modulus. Let Δt be calculated as in Eq.(8). As the stability region of the explicit time integration scheme is fixed, and Δt is inversely proportional to $\|\lambda_F\|$, then $\Delta t^{\text{ROM}} \geq \Delta t^{\text{FOM}}$. □

Remark 1 (Applicability to time-integration). Strictly speaking, Theorem 1 guarantees $\Delta t^{\text{ROM}} \geq \Delta t^{\text{FOM}}$ only when the convective field is identical for both FOM and ROM (i.e. $\mathbf{u} = \Phi\mathbf{a}$). In a practical time-integration scenario, the ROM trajectory $\mathbf{u}_r = \Phi\mathbf{a}(t)$ will deviate from the FOM solution $\mathbf{u}(t)$. Consequently, a rigorous inequality cannot be guaranteed for $t > 0$.

However, Theorem 1 serves as a strong theoretical proxy for the stability behavior of the ROM. Since the projection Φ inherently removes the high-frequency modes associated with the largest eigenvalues of $C(\mathbf{u})$, the inequality $\rho(C_r) < \rho(C)$ is expected to hold robustly in practice. The theorem thus provides the structural justification for the increased stability limits observed in numerical experiments, even in the presence of trajectory divergence.

4. Numerical experiments

In this section, the new adaptive timestepping method outlined in Algorithm 1 is tested for two different fluid flow test cases. First of all, the robustness of the method in a case without boundary conditions, namely the shear-layer roll-up, is presented. Moreover, the evolution of the maximum stable Δt for different numbers of modes is presented, and compared with the maximum stable Δt using the AlgEigCD. In the second case, the influence of non-homogeneous boundary conditions on the preservation of stability is considered for the unsteady wake behind an actuator disk [8]. In both test cases, the classical explicit fourth-order RK scheme is used in a two-dimensional incompressible Navier-Stokes solver [52, 53]. Both methods have been run for $M = [16, 32, 64, 128, 200]$ modes. Table 2 summarizes the methods used in this work.

4.1. Shear-layer roll-up

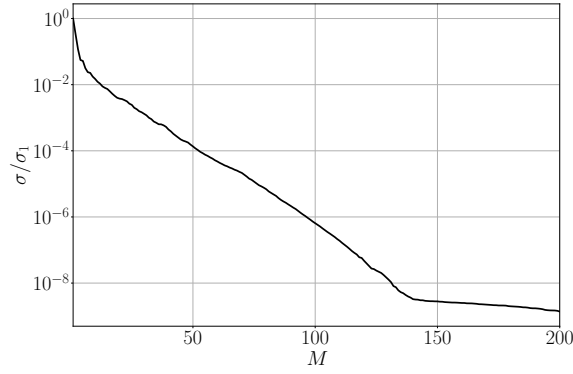
In this case, the roll-up of a shear layer has been simulated using a square domain of side length 2π with full-periodic boundary conditions. The initial conditions for the case are the following:

Table 2: Summary of the methods considered in this work.

| Case | Method | Description / Purpose |
|------|--------------|--|
| A | FOM+AlgEigCD | Full-order model with staggered AlgEigCD (Appendix B); used as reference. |
| B | ROM+RedEigCD | ROM with proposed self-adaptive timestep method. |
| C | ROM+constant | ROM with constant Δt ; used to compare accuracy of ROM+RedEigCD. |
| D | Best ROM | Best approximation ROM (Eq. (39)) with constant Δt ; used to verify $\Delta t_{\text{ROM}} > \Delta t_{\text{FOM}}$ throughout simulation. |

$$u_0(x, y) = 1 + \begin{cases} \tanh\left(\frac{y-\pi/2}{\delta}\right), & y \leq \pi, \\ \tanh\left(\frac{3\pi/2-y}{\delta}\right), & y > \pi, \end{cases} \quad v_0(x, y) = \epsilon \sin(x), \quad (38)$$

where $\delta = \pi/15$ and $\epsilon = 1/20$. The Reynolds number is 1000. The FOM discretization used for this case employs 100×100 finite volumes, with variable timestep computed using AlgEigCD (Appendix B). Snapshots have been extracted for $t = 0$ to $t = 20$ from Case A (Table 2). Figure 4 shows the decay of the singular values for this case.

Figure 4: Singular values for the Re=1000 shear-layer roll-up up to $M = 200$.

Moreover, note that even for the largest number of modes considered, $M = 200$, where the singular values have decayed up to $O(10^{-9})$, the number of degrees of freedom is notably reduced compared to those of the FOM, which is 3×10^4 , considering both x - and y - velocity components as well as the pressure. The simulation has been run for Case B (ROM+RedEigCD) with the number of modes previously stated and the evolution of Δt is compared with Case A.

Figure 5 (left) shows that the new self-adaptive timestepping method is effective in providing a larger timestep for the ROM than for the FOM, as expected from Theorem 1, as even for $M = 200$, the largest number of modes considered, the ratio is around 1, which is indicated in the plot with a horizontal thicker line. Depending on the current flow physics and number of modes of the ROM, this timestep can be up to 9 times larger than for the FOM, which significantly accelerates the simulation by notably reducing the number of timesteps required to reach the final time. Moreover, as shown in Figure 7, the accuracy of the ROM is not compromised by the use of RedEigCD.

Furthermore, Figure 5 (left) shows how the ratio between the timesteps obtained in Case B and Case A converges to 1 for increasing ROM dimension, as expected from Theorem 1, as the eigenvalues of the reduced operators interlace with those of the full-order operators. This is especially lucid for $M = 200$, where the singular values have decayed to $O(10^{-9})$, and the truncation errors between the ROM and the FOM (Figure 4) get closer to zero. Furthermore, note that at certain points, especially at the beginning of the simulation, the timestep ratio for $M = 200$ is slightly smaller than 1.

With regards to the time-evolution of the imaginary eigenbound (Figure 5, right), the expected behaviour as

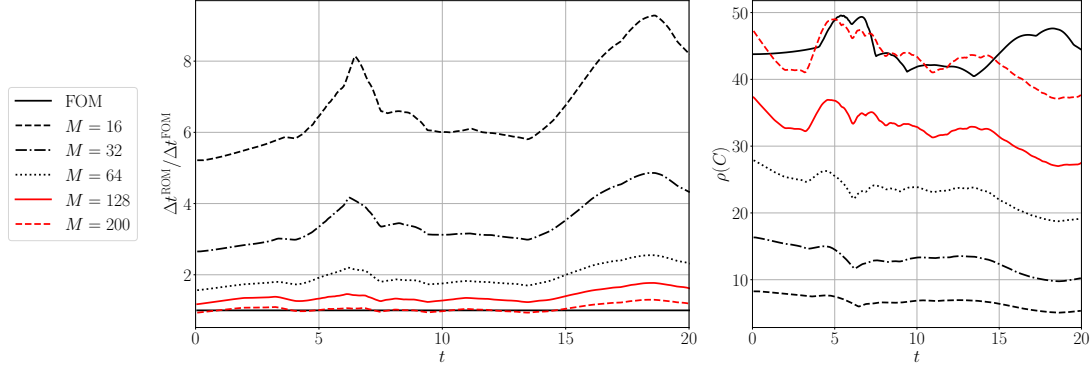


Figure 5: Timestep ratio between **Case B** and **Case A** up to $t = 20$ (left) and evolution of the imaginary eigenbound (right) for the roll-up of a shear-layer at $\text{Re} = 1000$.

theoretically derived in Section 3.2 holds: the eigenbound of the reduced convective terms steadily increases with an increase in the number of modes. For $M = 200$, however, in some points the imaginary eigenbound for the ROM is slightly larger than for the FOM. (Note that representing the time evolution for the diffusive operator has no relevance in this discussion, as it remains constant throughout the whole simulation.)

The reason for the mismatch with theory reported for $M = 200$ in Figure 5 is as follows. Section 3.2 considers that the given matrix at FOM level and its reduced counterpart are evaluated at the equivalent state vector \mathbf{u} . However, in a ROM simulation at a given t , the reduced velocity $\mathbf{u}_r(t) = \Phi \mathbf{a}(t)$ is not identical to its FOM counterpart, $\mathbf{u}(t)$, and therefore both velocity fields lead to non-identical convective operators. Given these differences, Lemma 2 acts as an approximation and thus it may happen that $\rho(C(\mathbf{u}(t))) \leq \rho(C(\mathbf{u}_r(t)))$ at a certain t when $\mathbf{u}(t) \neq \mathbf{u}_r(t)$.

Therefore, to test if the Δt at ROM level using the equivalent state vector is always larger than the one for the FOM actually holds, the best approximation ROM [8] should be used, which is defined as

$$\mathbf{a}_{\text{best}}(t) = \Phi^T \Omega \mathbf{u}(t), \quad (39)$$

which should fulfill Theorem 1 throughout the whole simulation as both $C(\mathbf{u})$ and $C_r(\mathbf{a}_{\text{best}})$ are evaluated at the equivalent state vector. Hence, the reduced convective and diffusive operators for every snapshot have been constructed, and the eigenbounds using the RedEigCD method have been computed. As shown in Figure 6, the result from Theorem 1 is indeed preserved throughout the whole simulation, with the Δt computed from the best approximation ROM for the largest number of modes, this being the most restrictive case.

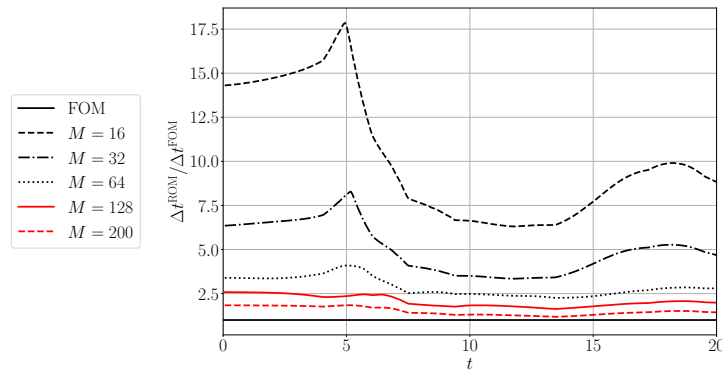


Figure 6: Timestep ratio between **Case D** and **Case A** for up to $t = 20$ for the roll-up of a shear-layer of $\text{Re} = 1000$.

Figure 7 shows that the errors for both **Case B** and **Case C** have the same magnitude regardless of the number of modes ($M = 16$, left; $M = 200$, right). Thus, the use of the self-adaptive timestepping methods as performed in these

cases does not significantly affect the accuracy of the ROM compared to the error of the best approximation ROM, as shown in Figure 7. In this case, Δt for Case C is set to 0.01, as in the test case from [8]. The used error is defined as follows,

$$\varepsilon(\mathbf{u}_{\text{test}}(t)) = \frac{\|(\mathbf{u}_{\text{test}}(t) - \mathbf{u}_A(t))\|_{\Omega_h}}{\|\mathbf{u}_A(t)\|_{\Omega_h}}, \quad (40)$$

where \mathbf{u}_{test} indicates the velocity field used to compute the error, i.e. \mathbf{u}_B , \mathbf{u}_C and \mathbf{u}_D ; \mathbf{u}_A corresponds to the snapshot at that given point in time, and $\|\cdot\|_X$ corresponds to the X -weighted L_2 norm.

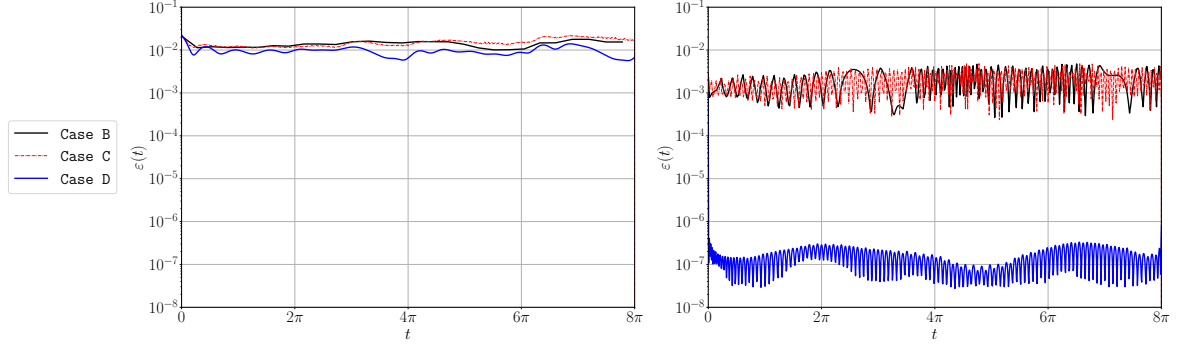


Figure 7: Error comparison of the ROM results for $M = 16$ (left) and $M = 200$ (right) in the shear-layer roll-up of $\text{Re} = 1000$ for Case B, C, and D.

In terms of efficiency, the ROM with $M = 64$ reduced the number of unknowns from 3×10^4 to 64, while simultaneously allowing timesteps up to almost 5 times larger than the FOM. This reduced the total number of timesteps, while the wall-clock time for each timestep was also reduced due to dimensionality reduction, thus having benefits from both factors. Figure 7 (left) shows that for $M = 16$ there is no loss of accuracy for the new self-adaptive timestepper (Case B) compared to Case C, which indicates that in this test case there is no loss of accuracy regardless of the number of modes, yet for this case the benefits of RedEigCD are greater, with potential gains of up to a factor of 9.

Moreover, the accuracy of estimating the eigenvalues for the convective term using RedEigCD has been tested against the actual eigenvalues. To do so, the reduced convective operator for the FOM at $t = 20$ has been constructed and its eigenbound has been precisely calculated and compared to the one estimated using RedEigCD, as reported in Section 4.3.

4.2. Flow through an actuator disk

In this case, the air flow around a wind turbine is modelled as in [22]. The simulation geometrical domain is $[0, 10] \times [-2, 2]$, with a time-dependent prescribed inlet velocity at the left boundary, as defined as follows,

$$u(0, y, t) = \cos(\alpha(t)), \quad v(0, y, t) = \sin(\alpha(t)), \quad \alpha(t) = \frac{\pi}{6} \sin\left(\frac{t}{2}\right). \quad (41)$$

The other boundaries correspond to an outflow condition [52, Section 6.4.2]. The wind turbine has been modelled using an actuator disk of diameter 1, placed at $(2, 0)$, which corresponds to a momentum sink modelled as a constant force $f = 0.25$ acting in the negative x -direction. The initial conditions for this case are

$$u_0(x, y) = 1, \quad v_0(x, y) = 0. \quad (42)$$

The Reynolds number is 100. The FOM discretization used for this case is 200×80 finite volumes, with variable timestep computed using AlgEigCD (Case A). The numerical tests performed correspond to those of Table 2. Snapshots have been extracted for $t = 0$ to $t = 8\pi$. Similarly to the roll-up of a shear-layer, the decay of the singular values is presented in Figure 8. Note that the decay follows the same trend as in Figure 4.

The new stability-aware self-adaptive timestepping method is effective in significantly increasing the timestep while maintaining stable simulations for non-homogeneous boundary conditions as shown in Figure 9 (left). The

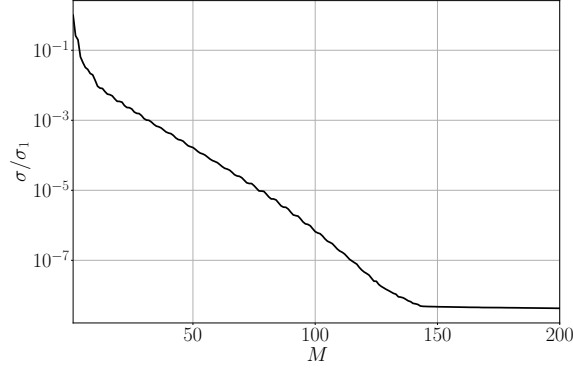


Figure 8: Singular values for the numerical simulation of an actuator disk of $Re = 100$ up to 200 modes.

obtained timestep for this case, depending on the flow conditions and the number of modes, can be up to 40 times larger, thus leading to significantly faster simulation times. Moreover, as expected from Section 3.2, the evolution of the timestep in the case of the actuator disk shows that for $M = 200$, for which the singular values do not decay anymore, the obtained timestep is marginally larger than the obtained for Case A. As can be seen in Figure 9 (right), the imaginary eigenbound is larger for larger ROM dimensions, analogously to the shear-layer roll-up testcase in Figure 5 (right). Note that in this case, the contribution of the boundary conditions appear in both the real and the imaginary term.

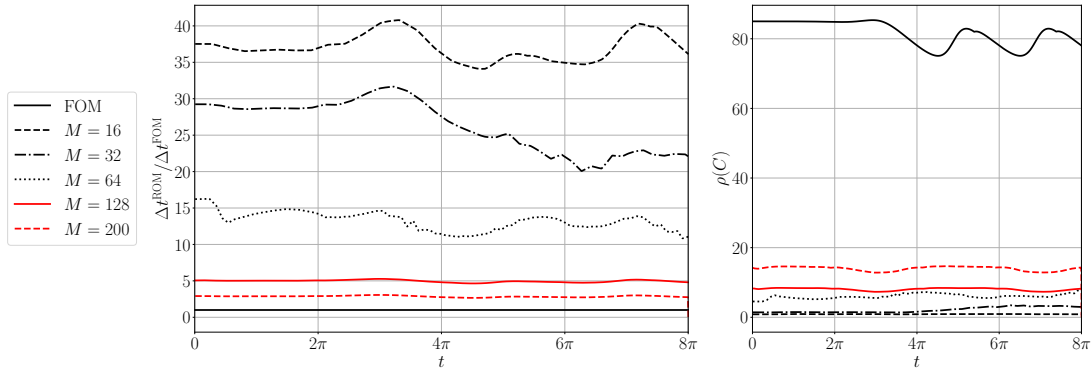


Figure 9: Timestep ratio between Case B and Case A up to $t = 100$ (left) and evolution of the imaginary eigenbound (right) in the numerical simulation of a wind field of $Re = 100$.

The magnitude of the ROM error, calculated with Eq.(40), is not affected by the variable Δt compared to the reference result from [8], where Δt was set to $4\pi/200$. As shown in Figure 10, the accuracy of the ROM+RedEigCD (Case B) is comparable to that of the ROM with constant Δt (Case C), for both $M = 16$ and $M = 200$. Note that the error for Case D (best approximation ROM) is significantly smaller than for Cases B and Case C, as expected.

4.3. Accuracy of the eigenbound estimates

The accuracy of the eigenvalue estimation using RedEigCD has been tested for both shear-layer roll-up as well as the actuator case. The results also include the eigenbounds obtained by applying Gershgorin's circle theorem directly to $a_i C_{r,i}$, which would replicate EigenCD for ROMs. Figure 11 presents the results.

In order to compute an overall error between the actual eigenvalues and the estimations, the following error is defined:

$$\varepsilon_{\text{est}} = \frac{\|\lambda_{a_i C_{r,i}} - \lambda_{\text{est}}\|_{\infty}}{\|\lambda_{a_i C_{r,i}}\|_{\infty}}, \quad (43)$$

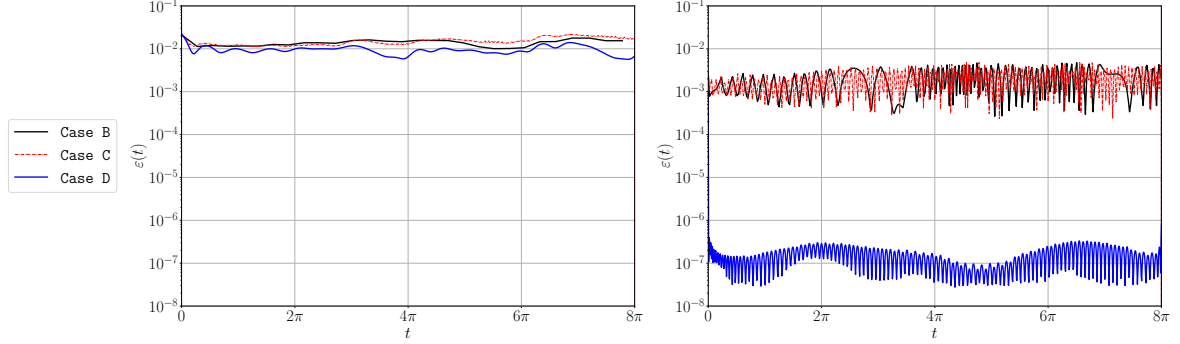


Figure 10: Error comparison of the ROM results for $M = 16$ (left) and $M = 200$ (right) in an actuator disk simulation with $Re = 100$ for **Case B**, **Case C**, and **Case D**.

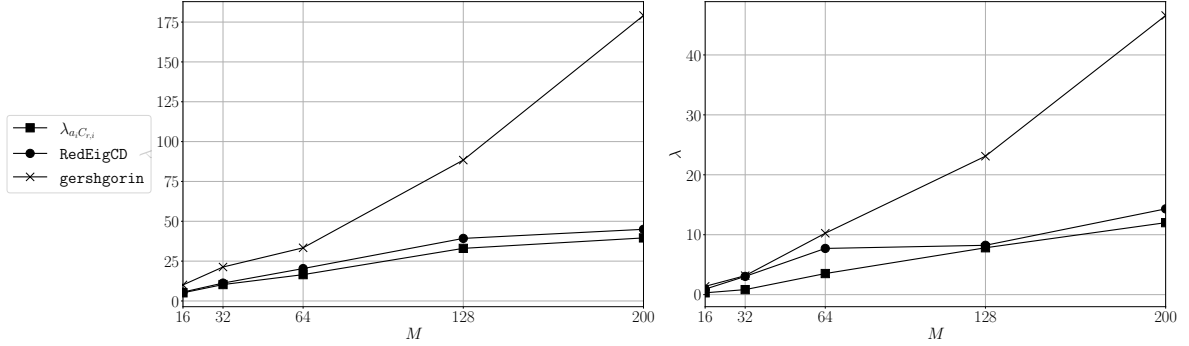


Figure 11: Comparison of the actual eigenvalues of the reduced convective operator at $t = 8\pi$ for the shear layer case of $Re=1000$ (left) and the actuator case of $Re=100$ (right) against the estimated eigenvalues using RedEigCD and the corresponding Gershgorin circles.

where $\lambda_{a,C_{r,i}}$ is the actual eigenbound of the Jacobian of the reduced convective operator at $t = 20$, and λ_{est} is the estimated eigenbound. The errors for RedEigCD are 0.158 and 0.349 for the shear-layer and actuator case, respectively. On the other hand, for the Gershgorin approximation, the errors are 3.53 and 2.88, respectively. Therefore, the estimation of eigenbounds for both cases using RedEigCD is significantly more accurate than the one obtained using Gershgorin's circle theorem.

5. Conclusion

In this paper, the application of self-adaptive timestepping for the time integration of a POD-Galerkin ROM for the incompressible Navier-Stokes simulations has been presented. The method is based on the conceptual ideas from EigenCD [6] and AlgEigCD [7], in which the eigenbound of the convective and diffusive operators is estimated in such a way that the eigenbound of the convection-diffusion operator can be placed on the boundary of the stability region of the explicit time integration scheme used.

Nonetheless, when the aforementioned methods would be applied directly to a ROM framework, they would require operations that scale with the FOM dimension. To avoid these operations, we have proposed a new methodology, RedEigCD, that can effectively estimate the eigenbound of reduced convective and diffusive operators. We extend upon the methodology applied by Sanderse [8], where the reduced convective operator is split into a quadratic and a linear contribution with the ROM coefficients, and utilized the sub-additivity of eigenbounds as well as Bendixson's rectangle. Thus, this allowed simplifying the method to a linear combination of the eigenbounds of the reduced convective operator, which is computed offline. On the other hand, the diffusive operator does not change in time. Therefore, its eigenbound can be computed exactly in an offline phase as well. The combination of these two computations, along with scaling the timestep as in [6, 7] with this eigenbound, forms the core of RedEigCD.

The presence of non-homogeneous boundary conditions that affect the linear term in the reduced convective term is also considered. Their interactions are modifying the structure of the matrix, breaking its skew-symmetry arising from the symmetry-preserving ROM that was applied. We proposed to address this by splitting this contribution into its symmetric and skew-symmetric parts, and adding them to the diffusive and convective terms, respectively.

The method has been tested in a fully-periodic shear-layer roll-up for up to $t = 20$, which tests the general aspects of the methodology while avoiding any boundary conditions. It has been shown that, in general, the Δt obtained for the ROM using RedEigCD is larger than the Δt at the FOM level, due to the interlacing of eigenvalues, which leads to smaller eigenbounds for the reduced counterparts. The benefits in timestep size for the ROM+RedEigCD for the shear-layer roll-up can be close to a factor of 10, depending on the number of modes used and the flow conditions. This leads to reduced simulation times due to the decreased number of timesteps needed.

Moreover, the method has been tested in a case with time-dependent boundary conditions. Therefore, the simulation of a wind field has been performed where the wind turbines are modelled using an actuator disk. As in the shear-layer roll-up, the obtained Δt with AlgEigCD for the FOM is consistently smaller than its counterpart for the ROM, proving the applicability of RedEigCD in the presence of time-dependent boundary conditions. In this case, the new self-adaptive timestepping method showcases a even larger improvement in timestep size compared to its FOM counterpart of up to a factor of 40 depending on the number of modes used and the flow conditions.

In both test cases, the obtained eigenbounds with the new method have been compared against the exact eigenbounds of the reduced operators as well as the estimated eigenbounds obtained by applying Gershgorin's circle theorem to the reduced operators. The method showed good agreement with the exact eigenbounds and outperformed Gershgorin's circle theorem estimates in both the shear-layer roll-up case and the actuator disk case. These results suggest that the method can provide accurate estimates of the eigenbounds of the reduced operators with and without non-homogeneous boundary conditions.

The present work has introduced RedEigCD, a stability-driven, self-adaptive timestepping framework that extends classical CFL and eigenvalue-based methods to reduced-order models of incompressible flow. Using the linear stability bounds derived from Poincaré's separation theorem, it has been shown both theoretically and numerically that the stable timestep achievable in ROMs is systematically larger than their FOM counterparts. This theoretical stability guarantee, however, relies on the convective fields of the ROM and FOM being identical. In practice, the ROM trajectory naturally deviates from the FOM. Nonetheless, the stability of the FOM is determined by its smallest scales (large eigenvalues), which correspond to the modes truncated by the projection. Therefore, our proof justifies this increased stability in the reduced set of equations.

Beyond its theoretical insight, RedEigCD maintains the computational scalability of reduced models by confining all eigenvalue computations to the offline stage and by avoiding any FOM-size operations during the online stage. This results in an algorithm with a complexity of $O(M)$, thus becoming negligible as the complexity of advancing the ROM in time is $O(M^3)$. The resulting algorithm thus provides a practical and generalizable timestep control mechanism for projection-based ROMs.

Future work will focus on the generalization of our method to the case where hyperreduction is employed for the convective terms, which would allow to reduce the online computational cost of the ROMs from $O(M^3)$ to $O(M^2)$. The main challenge will be to estimate the eigenbounds of the hyperreduced convective operator (the diffusive term remains unchanged). The practical performance of the method in more complex geometries and flow conditions should also be evaluated, but conceptually the method should be able to handle such situations. as it is general and can be applied to any flow configuration. Finally, the proposed RedEigCD framework can be extended to general non-quadratic problems by employing lifting transformations to recast the governing equations into a quadratic-bilinear form [54]. This approach eliminates non-quadratic nonlinearities, thereby restoring the algebraic structure to directly apply RedEigCD.

Acknowledgements

This work is supported by the *Ministerio de Economía y Competitividad*, Spain, SIMEX project (PID2022-142174OB-I00). J.P.-R. is also supported by the Catalan Agency for Management of University and Research Grants (AGAUR), 2022 FI_B 00810. H.R. and B.S. are supported by the project "Discretize first, reduce next" (with project number VI.Vidi.193.105 of the research programme NWO Talent Programme Vidi which is (partly) financed by the Dutch Research Council (NWO)).

Appendix A. Non-uniformly sampled Proper Orthogonal Decomposition of the snapshots matrix

The POD basis arises from the solution of the eigenvalue problem [43]

$$R\Phi_j = \lambda_j\Phi_j, \quad (\text{A.1})$$

where R is a correlation matrix between the velocity fields and Φ_j are the columns of the POD basis,

$$R = \frac{1}{T} \int_0^T \mathbf{u}(t)\mathbf{u}^T(t) dt, \quad (\text{A.2})$$

where T is the total time of sampling. As Δt is non-constant when performing an integration using AlgEigCD, the integral from Eq.(A.2) does not reduce to the classical XX^T correlation matrix typically used in POD. Instead, the integral yields

$$R = \frac{1}{T} \sum_{i=1}^m \mathbf{u}_i \mathbf{u}_i^T \Delta t_i, \quad (\text{A.3})$$

when using a suitable quadrature rule. Introducing $\Delta \in \mathbb{R}^{K \times K}$ as the diagonal matrix containing the timesteps normalized with T ($\Delta t_i/T$) from each step, Eq. (A.3) yields

$$R = X\Delta X^T. \quad (\text{A.4})$$

Let $\tilde{X} = X\Delta^{1/2}$, where performing the square root of Δ is straightforward given it is a diagonal matrix. Then, the classical POD optimization problem is obtained in such a way that $R = \tilde{X}\tilde{X}^T$.

To consider the weighted orthonormality condition, the weighted and unweighted problems are related by $\Phi = \Omega^{-1/2}\hat{\Phi}$, where $\hat{\Phi}$ stands for the solution of the unweighted problem. Therefore, the snapshot matrix is also related in such a way that $\hat{X} = \Omega^{1/2}\tilde{X} = \Omega^{1/2}X\Delta^{1/2}$. Hence, $\hat{\Phi}$ is a product of the SVD of \hat{X} , i.e.

$$\hat{X} = \hat{\Phi}\Sigma\P^*. \quad (\text{A.5})$$

Hence, the columns of $\hat{\Phi}$, denoted by $\hat{\Phi}_j$ correspond to the eigenvectors of $\hat{X}\hat{X}^T$. Thus, the procedure to obtain Φ is summarized as follows: (i) obtain snapshots of the velocity field to build X and as a consequence \hat{X} , (ii) perform the SVD of \hat{X} to obtain $\hat{\Phi}$ and as a consequence Φ , (iii) truncate Φ to the given number of modes M . For more details on this procedure, the reader is referred to [8].

Appendix B. Extending AlgEigCD to staggered grids

The derivation performed by Trias et al. [7] has been designed for general collocated and unstructured grids, making the methodology very versatile and applicable to practically any industrial application. Even though the method is developed to be applied to any convective scheme, it is tailored for a symmetry-preserving discretization [34] as all fields are computed at the same locations, thus ensuring that the duality of the gradient and the divergence that build the Laplacian operator is preserved when those are applied to the velocity field, together with the fact that for all velocity field components, the convective operator will be the same. However, in the case of a staggered grid, given the shift in the meshes devoted to the velocity field components, this duality is not exactly preserved [35]. Thus, the method cannot be generalized directly in this framework.

Before moving into the extension to staggered grids, it will become important to settle the base theorem used for AlgEigCD in order to simplify the estimates of the eigenbounds of operators to simple algebraic operations. To keep the idea from AlgEigCD [7], the same property is used:

Theorem 2. (Theorem 1 in [7]). Let $A \in \mathbb{R}^{n \times m}$ and $B \in \mathbb{R}^{m \times n}$ be rectangular matrices and $m \geq n$. Then, the square matrices $AB \in \mathbb{R}^{n \times n}$ and $A^T B^T \in \mathbb{R}^{m \times m}$ have the same eigenvalues except for the zero-valued ones.

In terms of the diffusive operator, a second-order symmetry-preserving operator can be built by concatenating two first-order operators [35, 55], which leads to

$$D = K\Lambda S, \quad (\text{B.1})$$

where $K \in \mathbb{R}^{N_V \times N_F}$ is a differencing matrix from staggered faces (N_F) to staggered cells (N_V), $\Lambda \in \mathbb{R}^{N_F \times N_F}$ corresponds to a diagonal matrix containing the diffusivities at the staggered faces, and $S \in \mathbb{R}^{N_F \times N_V}$ is a differencing matrix from staggered cells to staggered faces. Thus, from [7] it follows that a family of α -dependent matrices can be built using Theorem 2 such that their eigenbound is the same as the one from the diffusive term (Eq. (B.1)). Hence, applying Theorem 2 with $A = K\Lambda^\alpha$ and $B = \Lambda^{1-\alpha}S$,

$$\Lambda^\alpha K_h^T S_h^T \Lambda^{1-\alpha}. \quad (\text{B.2})$$

Therefore, the Gershgorin circle theorem can be applied straightaway to Eq. (B.2) as it will have the same eigenbound as the diffusive term, which leads to

$$\rho(D) \leq \max\{\text{diag}(\Lambda^\alpha) \circ |K^T S^T| \text{diag}(\Lambda^{1-\alpha})\}, \quad (\text{B.3})$$

where \circ denotes the Hadamard product, i.e., elementwise product.

The benefit of using this method instead of the Gershgorin circle theorem straight-away to D is that $|K^T S^T|$ can be build in a pre-process stage. Thus, every timestep, assuming Λ varies as in a LES framework, only a sparse matrix-vector product (SpMV) and possibly (if $\alpha \neq 0$) an elementwise vector-vector product (axty) should be performed, opposite to needing to rebuild the matrix every step, as for EigenCD [6].

With regards to the convective term, Sanderse [8] defines its construction in a staggered framework as

$$C(\mathbf{u}_s)\mathbf{u}_s = K((\Pi\mathbf{u}_s + \mathbf{y}_I) \circ (A\mathbf{u}_s + \mathbf{y}_A)), \quad (\text{B.4})$$

where $\Pi \in \mathbb{R}^{N_F \times N_V}$ interpolates the fluxes to the staggered faces, and $A \in \mathbb{R}^{N_F \times N_V}$ interpolates the velocities to the staggered faces. Moreover, $\mathbf{y}_A, \mathbf{y}_I \in \mathbb{R}^{N_F}$ apply the boundary conditions to the interpolated fields in order to account for them. However, \mathbf{y}_A can be dropped for the stability analysis as it does not have an associated volume. Thus, they would cancel out when the volume matrix is added to the equation. However, the interpolated boundary conditions vector \mathbf{y}_I is associated with faces and thus they should still be considered.

Thus, the convective term can be rewritten as

$$C(\mathbf{u}_s) = KFA, \quad (\text{B.5})$$

where $F = \text{diag}(\Pi\mathbf{u}_s + \mathbf{y}_I) \in \mathbb{R}^{N_F \times N_F}$ is a matrix containing the fluxes at the staggered faces in its diagonal. Trias et al. [7] shows that using Theorem 2 straight onto this definition does not give any benefit, as more entries are considered in the estimate, opposite to applying Gershgorin directly to $C(\mathbf{u}_s)$ [7]. Thus, let us recall the theorems used to develop the method.

Theorem 3. (Perron-Frobenius (PF) theorem, [56, 57]). Given an irreducible matrix $A \in \mathbb{R}^{n \times n}$ such that $[A]_{ij} \geq 0$, $\forall i, j$, it has a unique real and positive largest (in magnitude) eigenvalue $r \in \mathbb{R}^+$ and corresponding eigenvector with only positive entries, i.e.,

$$A\mathbf{v} = r\mathbf{v} \Rightarrow |\lambda| < r \text{ and } v_i > 0, \forall i \in \{1, \dots, n\}, \quad (\text{B.6})$$

where λ denotes any eigenvalue of A except r , and r is the Perron-Frobeniuseigenvalue.

Theorem 4. (Wielandt's theorem, [58]). Given a matrix A satisfying Theorem 3, and a matrix $B \in \mathbb{R}^{n \times n}$ such that $|[B]_{ij}| \leq [A]_{ij}$, $\forall i, j$. Then, any λ^B satisfies $|\lambda^B| \leq r$, where r is the PF eigenvalue of A .

Theorem 5. (Nikiforov's second Lemma, [59]). Let $A \in \mathbb{R}^{n \times n}$ be an irreducible, i.e. it is not similar via a permutation of a block upper triangular matrix, and a non-negative symmetric matrix $R \in \mathbb{R}^{n \times n}$ such that $[R]_{ii} = \sum_{j=1}^n [A]_{ij}$ and $[R]_{ij} = 0$ if $i \neq j$. Then,

$$\rho\left(R + \frac{1}{q-1}A\right) \geq \frac{q}{q-1}\rho(A), \quad (\text{B.7})$$

where the equality holds iff $[R]_{ii} = [R]_{jj}$ for any combination of i and j .

Hence, Theorem 4 may be used to relate the eigenbound of the convective operator and such from

$$A^C \equiv |K|F|A|, \quad (\text{B.8})$$

which corresponds to a symmetric positive matrix. Thus, by construction of A^C , its off-diagonal terms correspond to $2|C|$ as follows, $A^{C,off} = A^C - \text{diag}(\text{diag}(A^C)) = 2|C|$, while the rowsums of $A^{C,off}$ are equal to the diagonal terms of A^C given the skew-symmetry of C . Thus, $A^{C,off}$ satisfies PF, which implies it has a unique largest eigenvalue. Hence, applying Theorem 4, this can relate the eigenvalues of $|C|$ and those from C . Thus, Theorem 5 can be applied to $A^{C,off}$ and $\text{diag}(\text{diag}(A^C))$ such that with $q = 2$, the left-hand side becomes $\rho(A^C)$. This leads to

$$\rho(A^C) \stackrel{\text{Thm 5}}{\geq} 2\rho(A^{C,off}) = 4\rho(|C|) \stackrel{\text{Thm 4}}{\geq} 4\rho(C), \quad (\text{B.9})$$

as in [7], yet with the matrices having a different definition given their staggered nature. Now applying Eq. (B.9) together with Theorem 2 and Gershgorin circle theorem, this leads to

$$\rho(C) \leq \frac{1}{4} \max\{\text{diag}(|F|^\alpha) \circ \|K\|^T |A|^T \text{diag}(|F|^{1-\alpha})\}. \quad (\text{B.10})$$

However, as presented in [7], the relevant operators are scaled by Ω^{-1} . Therefore, the eigenbounds of both convective and diffusive operators read as

$$\rho(\Omega^{-1}D) \leq \max\{\text{diag}(\Lambda^\alpha) \circ |K^T \Omega^{-1} S^T| \text{diag}(\Lambda^{1-\alpha})\}, \quad (\text{B.11a})$$

$$\rho(\Omega^{-1}C) \leq \frac{1}{2} \max\{\text{diag}(|F|^\alpha) \circ \|K\|^T \Omega^{-1} |A|^T \text{diag}(|F|^{1-\alpha})\}. \quad (\text{B.11b})$$

The original version of AlgEigCD [7] showed that for a collocated solution of a Rayleigh-Bénard convection problem of $\text{Ra} = 10^{10}$, the most suitable value of α should be 0, as it minimizes the bounds for both diffusive and convective operator regardless of the mesh used. This is tested for a 2D shear-layer roll-up for four different uniform meshes with $N = \{10, 20, 40, 80\}$ divisions per direction. Figure B.12 shows that, while the eigenbounds for the diffusive operator are independent of α (left), the bounds for the convective operator are minimized for a value of α around 0, while still depending on the mesh size.

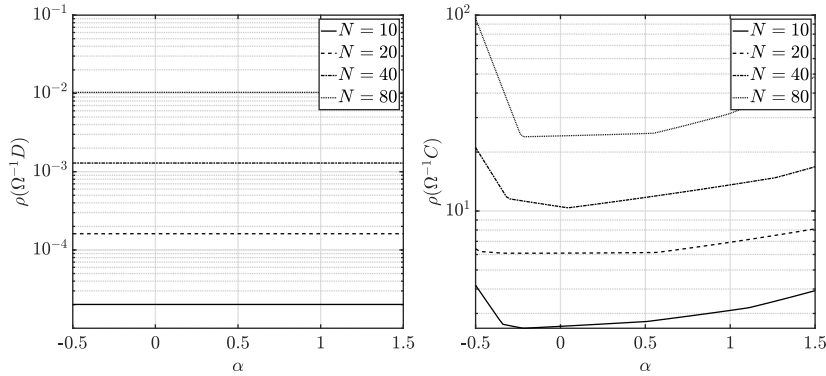


Figure B.12: Eigenbound estimation for the diffusive (left) and convective (right) operators for the roll-up of a shear-layer of $\text{Re} = 100$ with different mesh sizes as a function of α .

However, the use of $\alpha \neq 0$ introduces an additional operation in Eq.(B.12), doubling the number of operations required. Therefore, as the potential benefits of $\alpha \neq 0$ are almost negligible (Fig. B.12, right), $\alpha = 0$ is proposed in this case, which yields

$$\rho(\Omega^{-1}D) \leq \max\{|K^T \Omega^{-1} S^T| \text{diag}(\Lambda)\}, \quad (\text{B.12a})$$

$$\rho(\Omega^{-1}C) \leq \frac{1}{2} \max\{\|K\|^T \Omega^{-1} |A|^T \text{diag}(|F|)\}. \quad (\text{B.12b})$$

Appendix C. Jacobian of the convective term for a generic convection-diffusion equation

The momentum equation of the Navier-Stokes equations (Eq.(2b)) is a particular case of a generic convection-diffusion equation,

$$\frac{\partial \phi}{\partial t} + (\mathbf{u} \cdot \nabla) \phi = \frac{1}{\text{Pe}} \nabla^2 \phi + S_\phi, \quad (\text{C.1})$$

where the transported variable $\phi = \mathbf{u}$, $S_\phi = -\nabla p$ and the Péclet number $\text{Pe} = \text{Re}$. After spatial discretization with a finite-volume method, this generic convection-diffusion equation is written as

$$\Omega \frac{d\phi}{dt} + C(\mathbf{u}_c) \phi - D\phi + \Omega \mathbf{S} = \mathbf{0}, \quad (\text{C.2})$$

where \mathbf{u}_c is the discrete convecting velocity field, \mathbf{S} is the discrete source term and $\phi \in \mathbb{R}^{N_c}$ is the discrete generic variable, with N_c being the number of cells ($N_c \approx N_V/d$, being d the number of dimensions). Following Section 2.4, a POD-Galerkin approximation is obtained for both \mathbf{u}_c, ϕ . The former is equivalent to Eq.(10), while the latter reads as

$$\phi(t) \approx \phi_r(t) = \Theta \mathbf{b}(t), \quad (\text{C.3})$$

where $\Theta \in \mathbb{R}^{N_c \times M}$ is the projection matrix for ϕ , and $\mathbf{b}(t) \in \mathbb{R}^M$ is the coefficient vector for ϕ . Substituting both Ansatz (Eqs. (10), (C.3)) with Θ and Φ obtained with the procedure detailed in Appendix A and projecting it, the ROM equation reads as

$$\frac{d\mathbf{b}}{dt} = -\Theta^T C(\Phi \mathbf{a}_c) \Theta \mathbf{b} + \Theta^T D \Theta \mathbf{b} + \Theta^T \mathbf{S}. \quad (\text{C.4})$$

The reduced convective term now reads $\Theta^T C(\Phi \mathbf{a}_c) \Theta \mathbf{b}$, which following the procedure from Eq.(13) is rewritten as

$$C_r(\mathbf{a}_c, \mathbf{b}) = \Theta^T C(\Phi \mathbf{a}_c) \Theta \mathbf{b} = \underbrace{[\Theta^T C(\Phi_1) \Theta \dots C_{r,M}]}_{C_{r,1}} (\mathbf{a}_c \otimes \mathbf{b}) = \left(\sum_{i=1}^M a_{c,i} C_{r,i} \right) \mathbf{b}. \quad (\text{C.5})$$

The linear stability analysis for this convective term now requires linearizing the reduced convective term. Therefore, the Jacobian of the convective term reads as

$$J_C(\mathbf{a}_c) = \frac{\partial C_r(\mathbf{a}_c, \mathbf{b})}{\partial \mathbf{b}} = [C_{r,1} \dots C_{r,M}] (\mathbf{a}_c \otimes I_M) = \sum_{i=1}^M a_{c,i} C_{r,i}. \quad (\text{C.6})$$

References

- [1] E. Hairer, G. Wanner, S. P. Noersett, Solving Ordinary Differential Equations I, volume 8 of *Springer Series in Computational Mathematics*, Springer Berlin Heidelberg, Berlin, Heidelberg, 1993. URL: <http://link.springer.com/10.1007/978-3-540-78862-1>. doi:10.1007/978-3-540-78862-1.
- [2] J. C. Butcher, Numerical methods for ordinary differential equations, 3rd ed ed., Wiley, Chichester, West Sussex, 2016.
- [3] J. Dormand, P. Prince, A family of embedded Runge-Kutta formulae, *Journal of Computational and Applied Mathematics* 6 (1980) 19–26. URL: <https://linkinghub.elsevier.com/retrieve/pii/0771050X80900133>. doi:10.1016/0771-050X(80)90013-3.
- [4] E. Fehlberg, Klassische Runge-Kutta-Formeln fünfter und siebenter Ordnung mit Schrittwerten-Kontrolle, *Computing* 4 (1969) 93–106. URL: <http://link.springer.com/10.1007/BF02234758>. doi:10.1007/BF02234758.
- [5] R. Courant, K. Friedrichs, H. Lewy, Über die partiellen Differenzengleichungen der mathematischen Physik, *Mathematische Annalen* 100 (1928) 32–74. doi:10.1007/BF01448839.
- [6] F. X. Trias, O. Lehmkuhl, A Self-Adaptive Strategy for the Time Integration of Navier-Stokes Equations, *Numerical Heat Transfer, Part B: Fundamentals* 60 (2011) 116–134. URL: <http://www.tandfonline.com/doi/abs/10.1080/10407790.2011.594398>. doi:10.1080/10407790.2011.594398.
- [7] F. X. Trias, X. Álvarez Farré, A. Alsalti-Baldellou, A. Gorobets, A. Oliva, An efficient eigenvalue bounding method: CFL condition revisited, *Computer Physics Communications* 305 (2024). doi:10.1016/j.cpc.2024.109351, publisher: Elsevier B.V.
- [8] B. Sanderse, Non-linearly stable reduced-order models for incompressible flow with energy-conserving finite volume methods, *Journal of Computational Physics* 421 (2020). doi:10.1016/j.jcp.2020.109736, arXiv: 1909.11462 Publisher: Academic Press Inc.

- [9] C. Leblond, C. Allery, C. Inard, An optimal projection method for the reduced-order modeling of incompressible flows, *Computer Methods in Applied Mechanics and Engineering* 200 (2011) 2507–2527. URL: <https://www.sciencedirect.com/science/article/pii/S0045782511001617>. doi:10.1016/j.cma.2011.04.020.
- [10] R. Reyes, R. Codina, Projection-based reduced order models for flow problems: A variational multiscale approach, *Computer Methods in Applied Mechanics and Engineering* 363 (2020) 112844. URL: <https://www.sciencedirect.com/science/article/pii/S0045782520300256>. doi:10.1016/j.cma.2020.112844.
- [11] A. Prakash, Y. J. Zhang, Projection-based reduced order modeling and data-driven artificial viscosity closures for incompressible fluid flows, *Computer Methods in Applied Mechanics and Engineering* 425 (2024) 116930. URL: <https://www.sciencedirect.com/science/article/pii/S0045782524001865>. doi:10.1016/j.cma.2024.116930.
- [12] J. L. Lumley, The structure of inhomogeneous turbulence, in: *Atmospheric Turbulence and Wave Propagation*, Moscow, 1967, pp. 166–178.
- [13] L. Sirovich, Turbulence and the dynamics of coherent structures. I. Coherent structures, *Quarterly of Applied Mathematics* 45 (1987) 561–571. URL: <https://www.ams.org/qam/1987-45-03/S0033-569X-1987-0910462-6/>. doi:10.1090/qam/910462.
- [14] P. Holmes, J. L. Lumley, G. Berkooz, *Turbulence, Coherent Structures, Dynamical Systems and Symmetry*, 1 ed., Cambridge University Press, 1996. URL: <https://www.cambridge.org/core/product/identifier/9780511622700/type/book>. doi:10.1017/CB09780511622700.
- [15] A. Quarteroni, G. Rozza, Numerical solution of parametrized Navier–Stokes equations by reduced basis methods, *Numerical Methods for Partial Differential Equations* 23 (2007) 923–948. URL: <https://onlinelibrary.wiley.com/doi/10.1002/num.20249>. doi:10.1002/num.20249.
- [16] A. Manzoni, An efficient computational framework for reduced basis approximation and *a posteriori* error estimation of parametrized Navier–Stokes flows, *ESAIM: Mathematical Modelling and Numerical Analysis* 48 (2014) 1199–1226. URL: <http://www.esaim-m2an.org/10.1051/m2an/2014013>. doi:10.1051/m2an/2014013.
- [17] T. Lassila, A. Manzoni, A. Quarteroni, G. Rozza, *Model Order Reduction in Fluid Dynamics: Challenges and Perspectives*, in: *Reduced Order Methods for Modeling and Computational Reduction*, Springer International Publishing, Cham, 2014, pp. 235–273. URL: <http://link.springer.com/10.1007/978-3-319-02090-7>. doi:10.1007/978-3-319-02090-7.
- [18] D. Amsallem, C. Farhat, Stabilization of projection-based reduced-order models, *International Journal for Numerical Methods in Engineering* 91 (2012) 358–377. URL: <https://onlinelibrary.wiley.com/doi/abs/10.1002/nme.4274>. doi:10.1002/nme.4274, *eprint*: <https://onlinelibrary.wiley.com/doi/pdf/10.1002/nme.4274>.
- [19] E. Rezaian, M. Wei, A global eigenvalue reassignment method for the stabilization of nonlinear reduced-order models, *International Journal for Numerical Methods in Engineering* 122 (2021) 2393–2416. URL: <https://onlinelibrary.wiley.com/doi/abs/10.1002/nme.6625>. doi:10.1002/nme.6625, *eprint*: <https://onlinelibrary.wiley.com/doi/pdf/10.1002/nme.6625>.
- [20] Z. Wang, I. Akhtar, J. Borggaard, T. Iliescu, Proper orthogonal decomposition closure models for turbulent flows: A numerical comparison, *Computer Methods in Applied Mechanics and Engineering* 237–240 (2012) 10–26. URL: <https://linkinghub.elsevier.com/retrieve/pii/S0045782512001429>. doi:10.1016/j.cma.2012.04.015.
- [21] S. E. Ahmed, S. Pawar, O. San, A. Rasheed, T. Iliescu, B. R. Noack, On closures for reduced order models—A spectrum of first-principle to machine-learned avenues, *Physics of Fluids* 33 (2021) 091301. URL: <https://pubs.aip.org/pof/article/33/9/091301/1030870/On-closures-for-reduced-order-models-A-spectrum-of>. doi:10.1063/5.0061577.
- [22] H. Rosenberger, B. Sanderse, No pressure? Energy-consistent ROMs for the incompressible Navier–Stokes equations with time-dependent boundary conditions, *Journal of Computational Physics* 491 (2023) 112405. URL: <https://linkinghub.elsevier.com/retrieve/pii/S0021999123005004>. doi:10.1016/j.jcp.2023.112405.
- [23] R. B. Klein, B. Sanderse, Energy-conserving hyper-reduction and temporal localization for reduced order models of the incompressible Navier–Stokes equations, *Journal of Computational Physics* 499 (2024) 112697. URL: <https://www.sciencedirect.com/science/article/pii/S0021999123007921>. doi:10.1016/j.jcp.2023.112697.
- [24] C. Farhat, T. Chapman, P. Avery, Structure-preserving, stability, and accuracy properties of the energy-conserving sampling and weighting method for the hyper reduction of nonlinear finite element dynamic models, *International Journal for Numerical Methods in Engineering* 102 (2015) 1077–1110. URL: <https://onlinelibrary.wiley.com/doi/abs/10.1002/nme.4820>. doi:10.1002/nme.4820, *eprint*: <https://onlinelibrary.wiley.com/doi/pdf/10.1002/nme.4820>.
- [25] M. Barrault, Y. Maday, N. C. Nguyen, A. T. Patera, An ‘empirical interpolation’ method: application to efficient reduced-basis discretization of partial differential equations, *Comptes Rendus Mathématique* 339 (2004) 667–672. URL: <https://www.sciencedirect.com/science/article/pii/S1631073X04004248>. doi:10.1016/j.crma.2004.08.006.
- [26] S. Chaturantabut, D. C. Sorensen, A State Space Error Estimate for POD-DEIM Nonlinear Model Reduction, *SIAM Journal on Numerical Analysis* 50 (2012) 46–63. URL: <https://epubs.siam.org/doi/10.1137/110822724>. doi:10.1137/110822724, publisher: Society for Industrial and Applied Mathematics.
- [27] M. Ahmed, O. San, Stabilized principal interval decomposition method for model reduction of nonlinear convective systems with moving shocks, *Computational and Applied Mathematics* 37 (2018) 6870–6902. URL: <http://link.springer.com/10.1007/s40314-018-0718-z>. doi:10.1007/s40314-018-0718-z.
- [28] G. Stabile, F. Ballarin, G. Zuccarino, G. Rozza, A reduced order variational multiscale approach for turbulent flows, *Advances in Computational Mathematics* 45 (2019) 2349–2368. URL: <http://link.springer.com/10.1007/s10444-019-09712-x>. doi:10.1007/s10444-019-09712-x.
- [29] X. Li, Y. Xu, M. Feng, A Pressure-Stabilized Continuous Data Assimilation Reduced Order Model for Incompressible Navier–Stokes Equations, *Journal of Scientific Computing* 103 (2025) 10. URL: <https://link.springer.com/10.1007/s10915-025-02828-x>. doi:10.1007/s10915-025-02828-x.
- [30] C. Bach, L. Song, T. Erhart, F. Duddeck, Stability conditions for the explicit integration of projection based nonlinear reduced-order and hyper reduced structural mechanics finite element models, 2018. URL: <https://arxiv.org/abs/1806.11404>. doi:10.48550/ARXIV.1806.11404, version Number: 1.
- [31] G. Stabile, G. Rozza, Finite volume POD–Galerkin stabilised reduced order methods for the parametrised incompressible Navier–Stokes equa-

- tions, *Computers & Fluids* 173 (2018) 273–284. URL: <https://linkinghub.elsevier.com/retrieve/pii/S0045793018300422>. doi:10.1016/j.compfluid.2018.01.035.
- [32] I. Bendixson, Sur les racines d’une équation fondamentale, *Acta Mathematica* 25 (1902) 359–365. URL: <http://projecteuclid.org/euclid.acta/1485882119>. doi:10.1007/BF02419030.
- [33] C. Rao, Separation theorems for singular values of matrices and their applications in multivariate analysis, *Journal of Multivariate Analysis* 9 (1979) 362–377. URL: <https://linkinghub.elsevier.com/retrieve/pii/0047259X79900940>. doi:10.1016/0047-259X(79)90094-0.
- [34] F. X. Trias, O. Lehmkuhl, A. Oliva, C. D. Pérez-Segarra, R. W. Versteppen, Symmetry-preserving discretization of Navier-Stokes equations on collocated unstructured grids, *Journal of Computational Physics* 258 (2014) 246–267. doi:10.1016/j.jcp.2013.10.031, publisher: Academic Press Inc.
- [35] R. W. C. P. Versteppen, A. E. P. Veldman, Symmetry-preserving discretization of turbulent flow, *Journal of Computational Physics* 187 (2003) 343–368. doi:10.1016/S0021-9991(03)00126-8, publisher: Academic Press Inc.
- [36] A. J. Chorin, A numerical method for solving incompressible viscous flow problems, *Journal of Computational Physics* 2 (1967) 12–26. URL: <https://linkinghub.elsevier.com/retrieve/pii/002199916790037X>. doi:10.1016/0021-9991(67)90037-x, publisher: Elsevier BV.
- [37] B. Sanderse, B. Koren, Accuracy analysis of explicit Runge-Kutta methods applied to the incompressible Navier-Stokes equations, *Journal of Computational Physics* 231 (2012) 3041–3063. doi:10.1016/j.jcp.2011.11.028, publisher: Academic Press Inc.
- [38] S. D. Agdestein, B. Sanderse, Discretize first, filter next: Learning divergence-consistent closure models for large-eddy simulation, *Journal of Computational Physics* 522 (2025) 113577. URL: <https://www.sciencedirect.com/science/article/pii/S0021999124008258>. doi:10.1016/j.jcp.2024.113577.
- [39] E. Hairer, G. Wanner, Solving Ordinary Differential Equations II, volume 14 of *Springer Series in Computational Mathematics*, Springer, Berlin, Heidelberg, 1996. URL: <http://link.springer.com/10.1007/978-3-642-05221-7>. doi:10.1007/978-3-642-05221-7.
- [40] J. F. B. M. Kraaijevanger, Contractivity of Runge-Kutta methods, *BIT* 31 (1991) 482–528.
- [41] S. Gerschgorin, Über die Abgrenzung der Eigenwerte einer Matrix, *Bulletin de l’Académie des Sciences de l’URSS: Classe des sciences mathématiques et na* (1931) 749–754.
- [42] P. Benner, S. Gugercin, K. Willcox, A Survey of Projection-Based Model Reduction Methods for Parametric Dynamical Systems, *SIAM Review* 57 (2015) 483–531. URL: <http://epubs.siam.org/doi/10.1137/130932715>. doi:10.1137/130932715.
- [43] K. Kunisch, S. Volkwein, Optimal snapshot location for computing POD basis functions, *ESAIM: Mathematical Modelling and Numerical Analysis* 44 (2010) 509–529. URL: <http://www.esaim-m2an.org/10.1051/m2an/2010011>. doi:10.1051/m2an/2010011.
- [44] H. Rosenberger, Advances in Structure-Preserving Reduced Order Models for the Incompressible Navier-Stokes Equations, Master’s thesis, Technische Universiteit Eindhoven, Eindhoven, 2021. URL: <https://research.tue.nl/en/studentTheses/advances-in-structure-preserving-reduced-order-models-for-the-inc/>.
- [45] J. H. Wilkinson, The QR Algorithm for Real Symmetric Matrices with Multiple Eigenvalues, *The Computer Journal* 8 (1965) 85–87. URL: <https://academic.oup.com/comjnl/article-lookup/doi/10.1093/comjnl/8.1.85>. doi:10.1093/comjnl/8.1.85.
- [46] F. J. Corbató, On the Coding of Jacobi’s Method for Computing Eigenvalues and Eigenvectors of Real Symmetric Matrices, *Journal of the ACM* 10 (1963) 123–125. URL: <https://dl.acm.org/doi/10.1145/321160.321161>. doi:10.1145/321160.321161.
- [47] L. N. Trefethen, D. Bau, *Numerical Linear Algebra*, 1 ed., Society for Industrial and Applied Mathematics, 1997.
- [48] J. Baiges, R. Codina, S. Idelsohn, Explicit reduced-order models for the stabilized finite element approximation of the incompressible Navier-Stokes equations, *International Journal for Numerical Methods in Fluids* 72 (2013) 1219–1243. URL: <https://onlinelibrary.wiley.com/doi/10.1002/flid.3777>. doi:10.1002/flid.3777.
- [49] G. W. Stewart, *Matrix Algorithms: Volume II: Eigensystems*, Society for Industrial and Applied Mathematics, 2001. URL: <http://epubs.siam.org/doi/book/10.1137/1.9780898718058>. doi:10.1137/1.9780898718058.
- [50] J. R. Magnus, H. Neudecker, *Matrix differential calculus with applications in statistics and econometrics*, Wiley series in probability and statistics, 3rd ed ed., Wiley, Hoboken (N.J.), 2019.
- [51] Unitary equivalence and normal matrices, in: C. R. Johnson, R. A. Horn (Eds.), *Matrix Analysis*, Cambridge University Press, Cambridge, 1985, pp. 65–118. URL: <https://www.cambridge.org/core/books/matrix-analysis/unitary-equivalence-and-normal-matrices/01907C4F4E1B326B4E6E70CB316EFEB1>. doi:10.1017/CB09780511810817.004.
- [52] B. Sanderse, Energy-conserving discretization methods for the incompressible Navier-Stokes equations: application to the simulation of wind-turbine wakes, Ph.D. thesis, Technische Universiteit Eindhoven, 2013. URL: <https://research.tue.nl/en/publications/energyconserving-discretization-methods-for-the-incompressible-navierstokes-equations--application-to-the-simulation-of-.html>.
- [53] B. Sanderse, INS2D, 2018. URL: <https://github.com/bsanderse/INS2D>.
- [54] E. Qian, B. Kramer, B. Peherstorfer, K. Willcox, Lift & Learn: Physics-informed machine learning for large-scale nonlinear dynamical systems, *Physica D: Nonlinear Phenomena* 406 (2020) 132401. URL: <https://www.sciencedirect.com/science/article/pii/S0167278919307651>. doi:10.1016/j.physd.2020.132401.
- [55] B. Sanderse, R. Versteppen, B. Koren, Boundary treatment for fourth-order staggered mesh discretizations of the incompressible Navier-Stokes equations, *Journal of Computational Physics* 257 (2014) 1472–1505. URL: <https://linkinghub.elsevier.com/retrieve/pii/S0021999113006670>. doi:10.1016/j.jcp.2013.10.002, publisher: Elsevier BV.
- [56] O. Perron, Zur Theorie der Matrizen, *Mathematische Annalen* 64 (1907) 248–263. URL: <http://link.springer.com/10.1007/BF01449896>. doi:10.1007/BF01449896.
- [57] G. Frobenius, Über Matrizen aus nicht negativen Elementen, *Sitzung der physikalisch-mathematischen Classe* (1912) 456–477.
- [58] F. R. Gantmakher, *Applications of the theory of matrices*, Dover Publications, Mineola, N.Y., 2005. OCLC: 58720731.
- [59] V. Nikiforov, Chromatic number and spectral radius, *Linear Algebra and its Applications* 426 (2007) 810–814. URL: <https://linkinghub.elsevier.com/retrieve/pii/S0024379507002704>. doi:10.1016/j.laa.2007.06.005.